Converting Impulsive Kinetic Energy to DC Power for Self-Powered Microelectronics by Tunable, Nonlinear Vibration Energy Harvesters

Undergraduate Honors Thesis

Presented in Partial Fulfillment of the Requirements for Graduation with
Honors Research Distinction in the Department of Mechanical and Aerospace Engineering
of The Ohio State University

By

Inhyuk Park

Undergraduate Program in Mechanical Engineering

The Ohio State University

November 2017

Thesis Committee:
Ryan L. Harne, Advisor
Hanna Cho

ABSTRACT

Impulsive kinetic energies are abundant throughout natural and engineered environments including those energies due to human motion, pulsation of flow in pipes, vehicles driving over spanned bridges or speed bumps, and gusts of wind. Such impulsive energy is plentiful and collocated with many microelectronic systems that require small electrical power resources for their sustainment. As a result, researchers are investigating concepts of vibration energy harvesting using electromechanical oscillators that are sensitive to generate large electric energy conversion when excited by impulsive energy. Yet, a critical need exists to identify suitable energy harvesting systems that have high sensitivity to impulsive excitation in order to maximize the energy conversion capability. Recent studies have shown that nonlinear, bistable energy harvesters are generally sensitive to impulsive excitation. Motivated by the early findings, this research establishes and investigates a system of bistable energy harvesters driven by non-contact magnetic repulsion to convert piezoelectric beam strain into DC electrical power. Experimental and numerical investigations are conducted to characterize the effectiveness of the tunable, nonlinear vibration energy harvesting system to maximize the captured kinetic energy and to explore system configurations that optimize the DC power delivery. The results of this research reveal strategies for maximizing sensitivity of the vibration energy harvesting platform to the impulsive excitations via the magnetic force interactions and thus identify practical approaches for vibration energy harvesting in impulsive energy environments.

ACKNOWLEDGEMENTS

I first want to thank my advisor, Prof. Ryan L. Harne. Through him, I have learned a great knowledge on this research and attitude to treat research to obtain great results. This research would have not been accomplished without his encouragement and constant support.

I also wish to thank Prof. Hanna Cho for her help as my committee member.

All experiments presented in this research were conducted in the Laboratory of Sound and Vibration Research (LSVR), which is directed by Dr. Harne.

TABLE OF CONTENTS

List of Figures

1 Introduction

1.1 Motivation

Most wireless sensors have relied on batteries, but, they need to be recharged, replaced, and end up disposed which is costly and cumbersome. In addition, many structures may not have accessibility for humans to undertake such battery maintenance procedures. In structures like pipes or bridges, power supplies enabled by solar or wind energies may not even be feasible [1]. These challenges direct attention to other sustainable energies available in the environment of the structure under consideration and encourage study and development of microelectronic devices and sensors that may be powered by the local environment [2].

Importantly, many of these structures are in motion, so that kinetic energy in the form of vibration is available in the engineering system [3]. Capturing and converting this vibratory energy into a usable electric power resource is therefore a promising way to enable the functioning of microelectronics and wireless sensors [4]. Thus, vibration energy harvesting has recently become a promising field of study. Generally, vibration energy resources are a blend of harmonic, stochastic, and impulsive energies depending on the environment and context [5] [6] [7] [8]. Yet, impulsive energies have received less attention in the investigations of vibration energy harvesting principles, although there are numerous, common examples of impulsive kinetic energies. These include human activities and locomotion forces of walking and running, the motion of engineering infrastructures like that caused by vehicles driving over spanned bridges [bridges in parts with gaps separating parts], pulsation of flow in water/oil pipelines, and wind gusts on wind turbine blades [9] [10] [11] [12]. Impulsive excitations generate high amplitude vibration in structures in brief durations of time.

To gain knowledge on how to take advantage of these ambient energy sources, the deployment of suitable vibration energy harvester has become an essential field of study. Early research efforts developed linear energy harvesters that resonate at frequencies assumed to be associated with the ambient vibration [13]. This challenge led researchers to study nonlinearities that could be introduced to the energy harvesting devices to lead to large amplitude oscillations across broad ranges of frequencies that would result in large electrical energy conversion. To date, monostable Duffing [7] [14], impact [15] [6], bistable energy harvester designs have been popularly used for many studies.

Bistable energy harvesting devices have gained accelerated attention due to unique characteristics. The main characteristics of bistable stable energy harvester are two static equilibria that create a double-well potential energy profile as shown in Figure 1 [13]. Depending on the amount of energy input on the system, the oscillator creates different dynamic response. When the oscillator is subjected to low energy input, the inertial mass oscillates in the one of the potential well, which is called ‘intrawell’ vibration. When the input energy increases, the mass oscillates between two static equilibrium configurations, which is called ‘interwell’ vibration. This nonlinear dynamic characteristic is also called ‘snap-through’ vibration because bistable beams, which are a common realization of bistable structures, undergo a potentially violent snapping action from one stable equilibrium to the other in interwell-type dynamics. Snap-through in bistable vibration energy harvesters enable the oscillator to travel from one statically stable position to the

other stable position with high velocity [16] [17]. Thus, the transition can generate great displacement amplitude that leads to greater electrical power in the energy conversion. This research focuses on identifying strategies that may maximize sensitivity of the bistable energy harvester to impulsive excitation and to maximize DC power delivery.

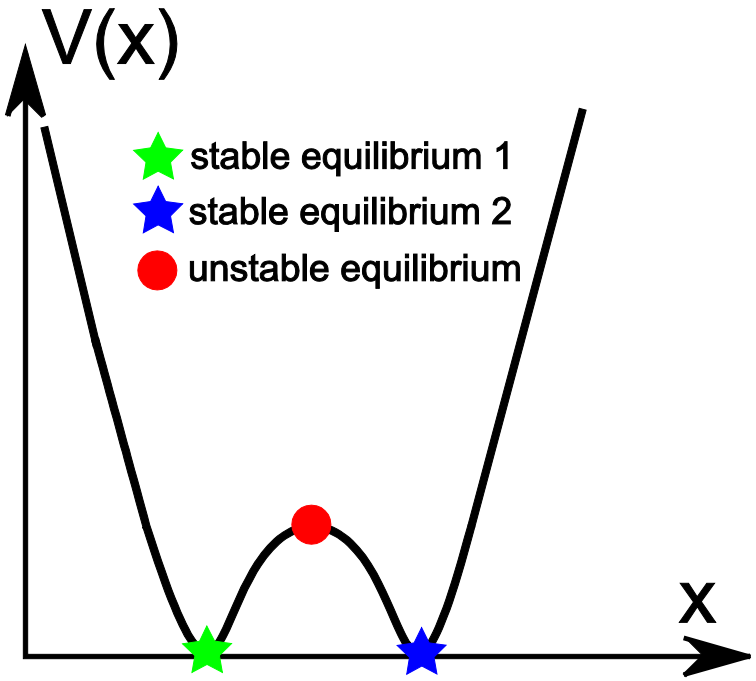

Figure 1. Double-well potential energy representative of a bistable oscillator

1.2 State-of-the-Art of Bistable Energy Harvesting Systems

Many early studies on vibration energy harvesting gave first attention to linear resonant harvesters driven by harmonic, single-frequency base excitations [18] [19]. Yet the broadband nature of ambient vibration energy encouraged studies of nonlinear energy harvesters that may be more sensitive to the practical energy available in the environment. These nonlinearities include monostability, impact, and bistability that broaden the bandwidth of frequencies at which large electrical energy conversion is achieved [7] [14] [20] [21]. The benefits of bistable oscillator have propelled researchers to develop different designs of bistable harvesters. Three ways of realizing bistable energy harvesting structures are common: magnetic repulsion, magnetic attraction, and axial compressive load [13]. In all cases, these influences act on a beam to which the mechanical response is coupled to electrical transduction, oftentimes via surface-bonded piezoelectric materials.

While much research has been directed to study nonlinear vibration energy harvesters subjected to harmonic and stochastic vibration forms, relatively few investigations have considered impulsive excitation. A recent study found that bistable vibration energy harvester have high promise for energy conversion when

subjected to impulsive inputs due to large amplitude dynamics that may be triggered for effective AC power delivery [11] [22] [23] [24] [25]. Thus, exploiting bistable energy harvesters have provided opportunity to deliver high sensitivy to impulsive excitaions and capture more vibration energy as electrical power [10].

1.3 Problem statement

Researchers have sought better understating on vibration energy harvesters under impulsive excitation. Among many studies, magnetic forces employed in bistable vibration energy harvester have played important role due to its characteristic of tunable magnetic forces to transfer impulsive energies avoiding physical contact to the harvesters which may cause damage to the system [26]. Along with experimental development, analytical approach to predict dynamic response to impulsive excitation has also been investigated [27]. Due to characteristics of the magnet's multi-directional force transmission regardless of uni-directional input force, magnetically coupled bistable beams are investigated along with bi- and tri-directional energy harvester using magnetic repulsion [28] [29]. Depending on the displacement of the fixed magnets in those systems, investigation on dynamic response using multi stable equilibria characteristics of single energy harvester beam has been focused for better energy conversion performance. Yet, there is still need of understanding of the characteristics of nonlinear magnetic forces under impulsive excitation and need to find strategies to maximize capture of kinetic energy for electrical energy conversion. This lack of the knowledge prevents developing and harnessing nonlinear vibration energy harvester enhanced by tunable magnet forces.

1.4 Research goal

The goal of this research is to obtain knowledge for characteristics of nonlinear multidirectional energy harvester under impulsive excitation. To achieve this goal, a coupled bistable vibration energy harvester system is designed and tuned by non-contact magnetic forces. Using a fabricated proof-of-concept device platform, experimental and numerical investigations are conducted to characterize the effectiveness of the tunable, nonlinear vibration energy harvesting system to convert impulsive input energy into DC electrical power. The investigations also seek knowledge on how to maximize the captured kinetic energy by system configurations and impulsive input properties that optimize the DC power delivery. The results of this research are assessed to identify strategies for maximizing sensitivity of the vibration energy harvesting platform to the impulsive excitations.

1.5 Overview of thesis

This thesis is organized as follows. Chapter 2 discuss the experimental setup of the coupled bistable vibration energy harvesting structure and describes the governing equations of magnetic forces, motion for this platform, and the energy conversion. Chapter 3 describes the data acquisition equipment and experiment method used for investigation of this research including structural parameters. Chapter 4 presents the experimental results and analytically discuss the insight on the results. Chapter 5 summarize the important discoveries of this research and propose prospective future investigation.

2 Designing and modeling of magnetically coupled energy harvesting system

2.1 Built-up bistable structure of magnetically coupled beams

In the previous research on magnetically coupled bistable energy harvester system, a magnet attached to the tip of an elastic beam coupled with another fixed magnet have shown the full range of bistable dynamic behaviors [16] [26]. The bistable beam exhibits multiple stable equilibria depending on the distance between the magnets. To harness the multi-directional magnetic forces for energy efficiency, this research investigate a magnetic repulsion energy harvester structure consisting of one fixed magnet, two elastic beams with magnets attached on the tips. Each spring steel beam (E = 200 GPa, ρ = 7800 kg/m^3, L = 3.9 mm, W = 1.3 mm, t = 0.26 mm) is clamped by an aluminum mount at one end and on the opposite end an aluminum magnet holder with neodymium magnet is attached. From here on, each magnet is referred to as "magnet 1" and "magnet 2" as labeled in Figure 2. A magnet fixed on the aluminum fixture is also referred as "magnet 3". Based on the magnetic polarization, magnets are positioned to transmit repulsive magnetic force to each other as shown in Figure 2(b). According to magnet configuration, the magnets 1 and magnet 2 create repulsive forces while the magnet 1 and magnet 3 create attractive force. The same poles of the magnet 1 and magnet 2 create repulsive force that create multistable positions of the cantilevered beam 2. For electrical energy conversion from AC to DC voltage, diode bridge rectifiers and smoothing circuits are connected to the outputs of the PVDF beams.

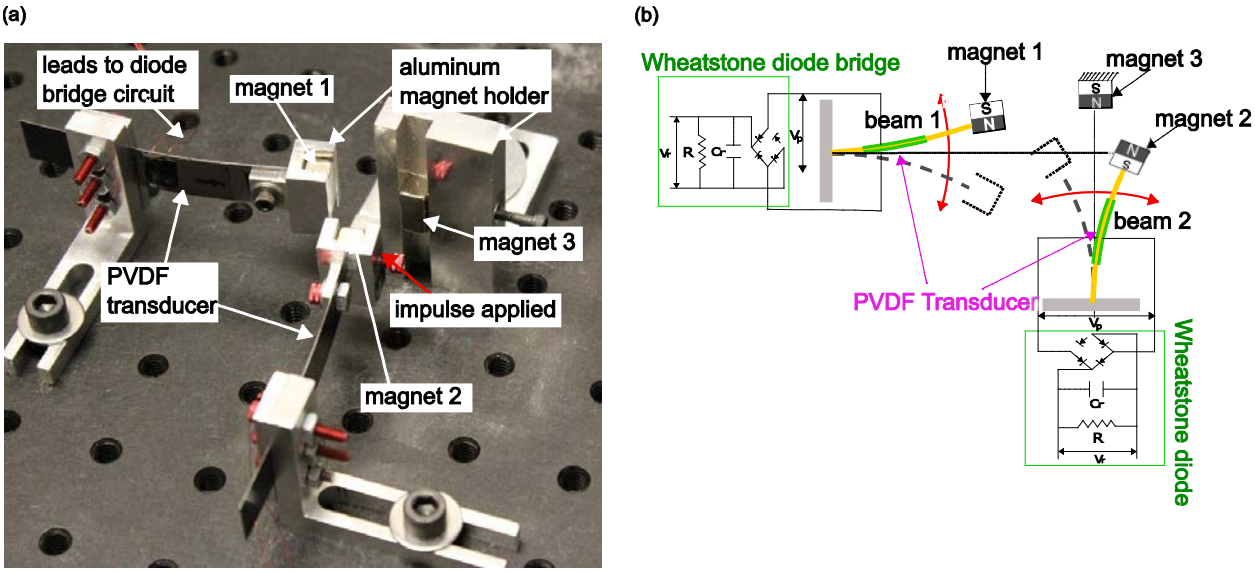

Figure 2. (a) Photograph of experimental energy harvester composition and location where impulses are applied. (b) Top view schematics of energy harvester platform and rectifier circuits.

The setup provides sufficient space to adjust the structural design, to tune structural properties, which makes it feasible to conduct parameter studies. For example, the aluminum frames for beam 2 move along the channels to adjust the distance between the magnet 1 and magnet 2 as shown in Figure 2. The aluminum frame for beam 1 moves within the channel on the frame to adjust relative distances to both magnet 2 and magnet 3. This adjustment of magnet 1 position optimizes the repulsive magnetic force and minimize

attractive force by magnet 3. The magnet fixture for the magnet 3 move multi direction within the square shaped channel on the frame to cooperate with distance to magnet 1 and magnet 2.

2.2 Governing equations for magnet displacement and magnetic force

To cover the wide range of parameter study and obtain more insight than that obtained through experiment, the model for this research is formed. Using the previously derived governing equation of motion of the archetypal bistable structure using Newton's and Kirchhoff's laws [30], the governing equations of motion for the magnetically coupled nonlinear energy harvester system was derived as

$$m_1\ddot{x}_1 + c_1\dot{x}_1 + k_{11}x_1 + k_{31}x_1^3 + \alpha_1 v_{p1} = F_{21} + F_{31} \tag{1a}$$

$$m_2\ddot{x}_2 + c_2\dot{x}_2 + k_{12}x_2 + k_{32}x_2^3 + \alpha_2 v_{p2} = F_{32} + F_{12} \tag{1b}$$

$$C_{pi}\dot{v}_{pi} + I_i = \alpha_i\dot{x}_i, (i = 1,2) \tag{1c}$$

where, x_1 and x_2 represent the lowest order generalized translational displacements of magnets on the cantilever beam 1 and 2, respectively; m_1 and m_2 represent the lumped mass of each cantilever beam including the magnet holder and tip magnet; c_i, k_{1i}, k_{3i} $(i = 1,2)$ are the viscous damping, linear stiffness, and nonlinear stiffness of beam 1 and 2; $\alpha_i (i = 1,2)$ denote the electromechanical coupling effects for the beams; $v_{pi} (i = 1,2)$ denote the AC voltages from output of PVDF beams; $C_{pi} (i = 1,2)$ denote the internal capacitances of the PVDF beams; overdot operation represent differentiation respect to time t.

$$I_i(t) = \begin{cases} C_{ri}\dot{v}_{ri} + \dfrac{v_{ri}}{R_i}; \text{ if } v_{pi} = v_{ri} \\ -C_{ri}\dot{v}_{ri} - \dfrac{v_{ri}}{R_i}; \text{ if } v_{pi} = -v_{ri}, (i = 1,2) \\ 0; \text{ if } |v_{pi}| < v_{ri} \end{cases} \tag{2}$$

$I_i(t)(i = 1,2)$ denote the alternating currents from the PVDF beams under assumption of the rectifiers being perfect; $v_{pi} (i = 1,2)$ are the AC voltages as used in the equation (1); $v_{ri} (i = 1,2)$ are the DC voltages; C_{ri} and $R_i (i = 1,2)$ denote the smoothing capacitors and load resistances, respectively.

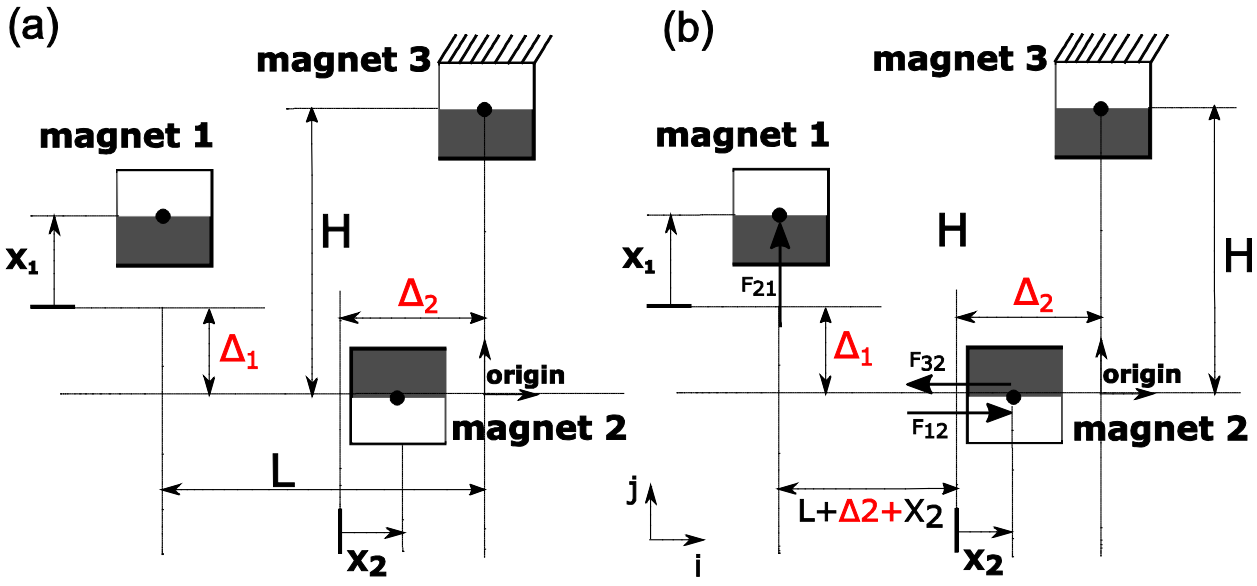

Figure 3. Detailed schematics of coordinate system a) Spacing parameter and magnet distances with center offset. b) Magnetic force vectors with magnet spacing parameter

To obtain the forces in the equations (1a and 1b), the magnetic forces are obtained acting on each magnets based on derived equation for two magnetic dipoles model [31]. The magnetic forces, $F_{mn,}$ demonstrated in Figure 3 represent the magnetic forces acting on magnet n by the dipole effect created by magnet m along transverse direction on either $\hat{\imath}$ or $\hat{\jmath}$ axis.

The magnetic forces acting on each magnet from different transverse directions are

$$\underline{F}_{21} = -\frac{3\mu_0 M_1 V_1 M_2 V_2}{4\pi}\frac{(L+x_2+\Delta_2)\left(-4(x_1+\Delta_1)^2+(L+x_2+\Delta_2)^2\right)}{\left((x_1+\Delta_1)^2+(L+x_2+\Delta_2)^2\right)^{7/2}}\hat{\imath} + \frac{3\mu_0 M_1 V_1 M_2 V_2}{4\pi}\frac{(x_1+\Delta_1)\left(-2(x_1+\Delta_1)^2+3(L+x_2+\Delta_2)^2\right)}{\left((x_1+\Delta_1)^2+(L+x_2+\Delta_2)^2\right)^{7/2}}\hat{\jmath} \quad (3a)$$

$$\underline{F}_{31} = -\frac{3\mu_0 M_1 V_1 M_3 V_3}{4\pi}\frac{L\left(-L^2+4(-H+x_1+\Delta_1)^2\right)}{\left(L^2+(-H+x_1+\Delta_1)^2\right)^{7/2}}\hat{\imath} + \frac{3\mu_0 M_1 V_1 M_3 V_3}{4\pi}\frac{(-H+x_1+\Delta_1)\left(-3L^2+2(-H+x_1+\Delta_1)^2\right)}{\left(L^2+(-H+x_1+\Delta_1)^2\right)^{7/2}}\hat{\jmath} \quad (3b)$$

$$\underline{F}_{12} = \frac{3\mu_0 M_1 V_1 M_2 V_2}{4\pi} \frac{\left(L + x_2 + \Delta_2\right)\left(-4\left(x_1 + \Delta_1\right)^2 + \left(L + x_2 + \Delta_2\right)^2\right)}{\left(\left(x_1 + \Delta_1\right)^2 + \left(L + x_2 + \Delta_2\right)^2\right)^{7/2}} \hat{i} -$$
$$\frac{3\mu_0 M_1 V_1 M_2 V_2}{4\pi} \frac{\left(x_1 + \Delta_1\right)\left(-2\left(x_1 + \Delta_1\right)^2 + 3\left(L + x_2 + \Delta_2\right)^2\right)}{\left(\left(x_1 + \Delta_1\right)^2 + \left(L + x_2 + \Delta_2\right)^2\right)^{7/2}} \hat{j} \tag{3c}$$

$$\underline{F}_{32} = \frac{3\mu_0 M_2 V_2 M_3 V_3}{4\pi} \frac{\left(x_2 + \Delta_2\right)\left(4H^2 - \left(x_2 + \Delta_2\right)^2\right)}{\left(\left(x_2 + \Delta_2\right)^2 + H^2\right)^{7/2}} \hat{i} +$$
$$\frac{3\mu_0 M_2 V_2 M_3 V_3}{4\pi} \frac{H\left(-2H^2 + 3\left(x_2 + \Delta_2\right)^2\right)}{\left(\left(x_2 + \Delta_2\right)^2 + H^2\right)^{7/2}} \hat{j} \tag{3d}$$

Where L and H represent spacing parameters respecting the reference coordinate system; Δ_1 represents the center offset distance between magnet 1 and magnet 2; Δ_2 represents the center offset distance between magnet 2 and magnet 3; μ_0 is the permeability constant, $4\pi \cdot 10^{-7}$ N/A^2; M_i(i=I,2,3) are magnetization; V_i(i=1,2,3) are magnet volume of each magnet.

The governing equations presented above are used to predict the behavior and electrodynamic response of the magnetically coupled nonlinear energy harvesting system subjected to impulsive excitation. After system parameter identification for the energy harvesting system used in this research, this model is utilized to generate various compatible simulation results.

3 Experimental and Simulation Methods

3.1 Sensors, equipment, and data acquisition methods

The absolute cantilever tip displacement is measured by a laser displacement sensor (micro Epsilon ILD-1700 laser) mounted on the same table as the harvester platforms as shown in Figure 4. This sensor is located perpendicular to the magnet holder. The laser displacement used in this research is to measure the initial velocity of the beam that is excited by the impulsive input. The PVDF transducers are attached on the both side of each beam to convert kinetic energy to electrical energy in form of AC voltage. The PVDF transducers are located nearby where the beams are clamped to maximize the energy conversion due to the increase bending strain near to the clamp position. The AC voltage is converted to DC voltage by the diodes in the bridge . All channels of data are recorded at a sampling frequency of 2048 Hz and digitally filtered by low-pass filter below 200 Hz. To validate the energy harvesting system model and investigate further on the system, governing equations derived in the previous section are used for numerical simulation using Runge Kutta numerical integration. The parameters used for the simulation are listed in Table 1. Codes used in the experiment post-processing and simulation are provided in the Appendix.

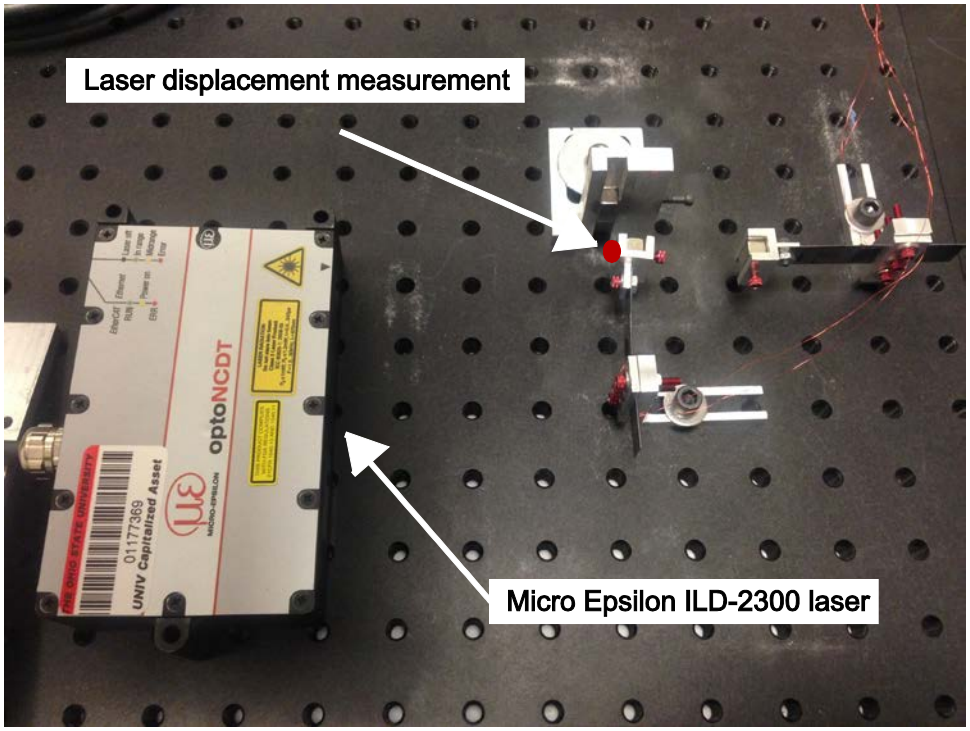

Figure 4. Photograph of laser displacement sensors and energy harvesters

3.2 Experiment overview

To investigate and obtain comprehensive understanding the energy harvester system under impulsive excitations, different kinds of experiment methods are approached to generate energy output. Impulsive excitations are characterized by two parameters: initial velocity and direction of excitation. The configuration of the energy harvesting platform is varied by the parameter L and H, the distances between

magnets as in Figure 2. Thus, in order to characterize the response of the energy harvester, combination of these parameters are experimentally tested. Before the dynamic response test, the center offsets of magnets 1 and 2 that create the effective magnetic forces acting on each magnet are measured. After the center offsets are decided, L sweep is conducted during which the center offsets of magnets 1 and 2, and H, the distance between magnets 2 and 3 are fixed. The L sweep is conducted with range of which both beams are dynamically response when beam 2 was excited by impulsive excitations (L from 27mm to 31mm). The L sweep is chosen to see how distance between magnets 1 and 2 influence on both static equilibria and dynamic response of the beam 1 and beam 2.

As similar to L sweep, H sweep is also conducted during which the center offsets of the magnets 1 and 2, and L, distance between magnet 1 and magnet 3, are fixed. The distance L is chosen, which transmits the dynamic forces between magnets 1 and 2 efficiently when the beam 2 is impulsively excited. The H sweep is chosen to observe how distance between magnets 2 and 3 influence on the bistability of the beam 2 and the dynamic response of the both beams 1 and 2.

Multi-direction excitation is conducted during which all variables for the configuration of the energy harvester are fixed. In these experiments, beam 1 and beam 2 are excited with impulsive input respectively for separate tests to investigate the dynamic response of the energy harvesting system when different direction of impulsive excitation is applied.

3.3 Impulsive excitation direction and initial position of beam

The coupled two energy harvester beams deliver more complicated configuration than a single harvester beam. Different direction of impulsive excitation on the beam may cause different dynamic response of the harvester beams. In order to characterize the dynamic response of the cantilever beams, all the impulsive excitations are constantly applied to same direction in each experiment test. In addition to constant direction, impulsive excitations are provided at the different static equilibrium positions of the beams, especially when the beam 2 have bistability as shown in Figure 5.

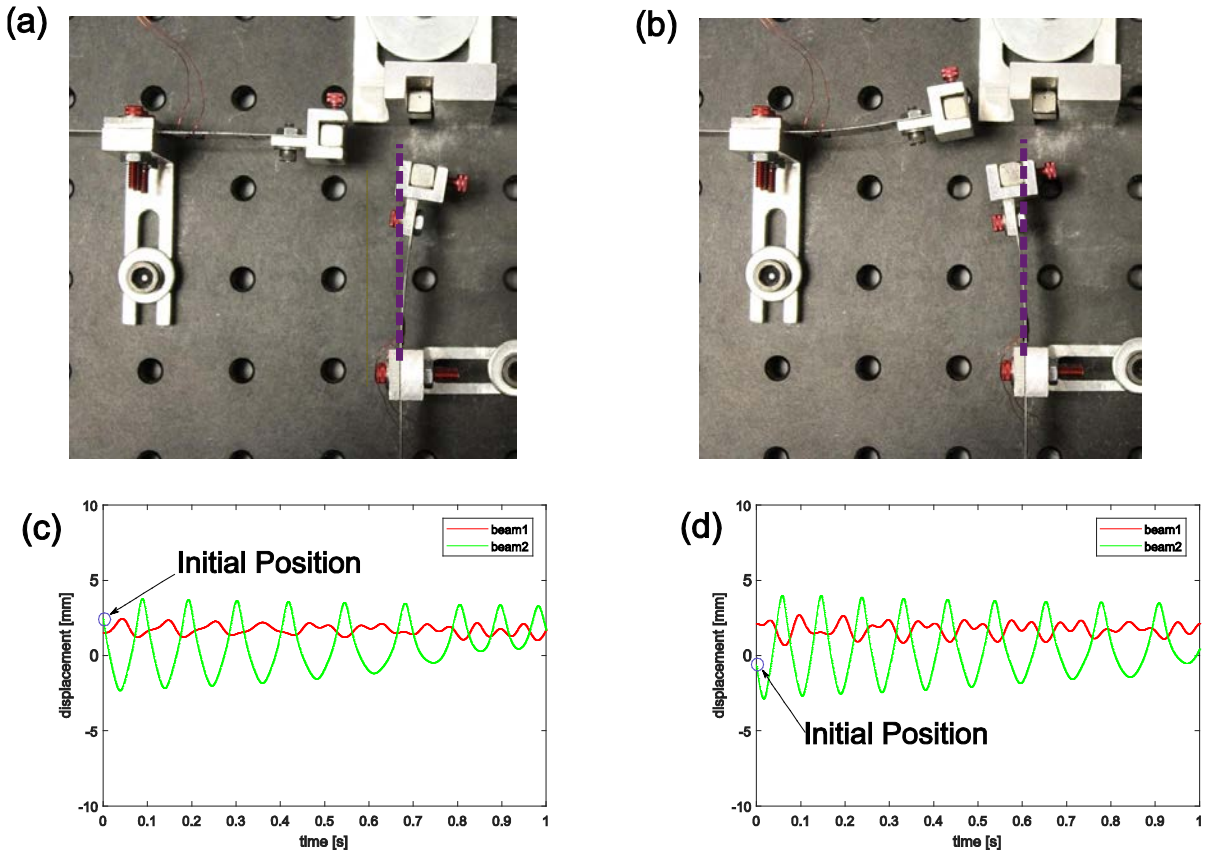

Figure 5. Photograph of bistability in the harvesting system (a) Magnet 2 located in a static equilibrium far from magnet 1. (b) Magnet 2 located in a static equilibrium close magnet 1

3.4 Structural parameters

As the governing equations in Section 2.2 demonstrate, there are 14 different kinds of parameters for the coupled energy harvesters. In order to determine those parameters, system identification is undertaken using the experimental system. The natural frequency and the damping ratio of cantilever beam are measured by the ring-down test. Each beam is separated individually from coupled setup. Then the beam is softly impacted at the tip to have free damping response as shown Figure 6. The log decrement method is used to calculate the linear natural frequency and damping ratio.

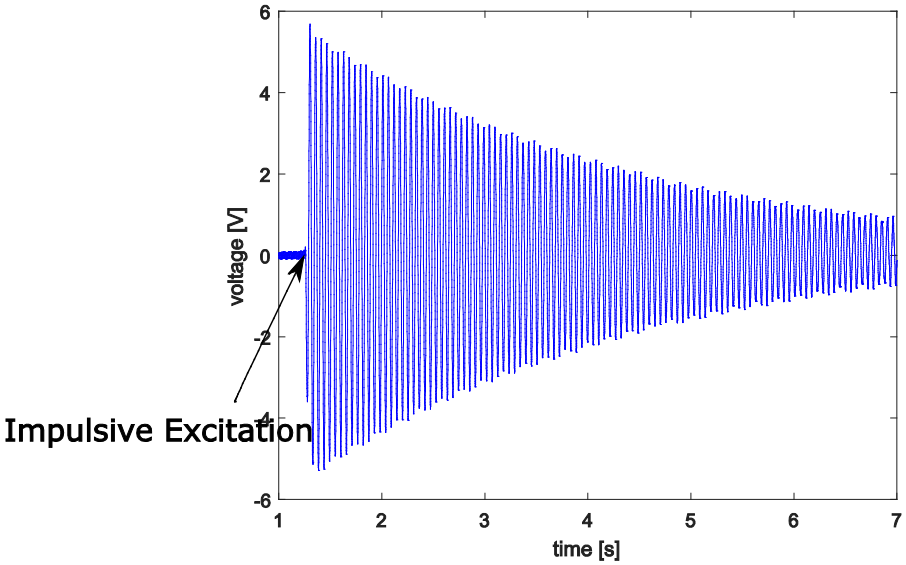

Figure 6. Free damping response from ring-down test. This test was conducted on beam 2 individually

Once the linear natural frequency and damping ratio for beam have been determined, the viscous damping constant, c_i, is calculated by

$$c_i = 2\zeta\omega_n m_i \tag{4}$$

where, ζ is the damping ratio; ω_n denote for the natural frequency of the beam; m_i is the effective mass. Other parameters in Table 1 are experimentally identified.

Table 1. Identified structure parameters, i = 1, 2

m_i [g]	c_i [N.s/m]	k_{1i} [N/m]	k_{3i} [MN/m^3]	ρ_i [kg/m^3]	A_i [mm^2]	α_i [mN/V]
7.0	0.008	60	6	3500	44.4	0.075
C_{pi} [nF]	C_{ri} [μF]	R_i [MΩ]	M_1 [MA/m]	M_2, M_3 [MA/m]	V_1, V_2, V_3 [cm^3]	
0.278	0.29	10	1.18	1.25	0.512	

4 Results and Discussions

4.1 Study of potential energy profiles

The energy harvesting system is highly sensitive to the nonlinear magnetic forces between magnet, which couple the motions of the two piezoelectric cantilever beams. The stable equilibria of the harvester beams vary by the distance between the magnets, which means the static magnetic forces vary depending on the spacing. To study characteristics of magnetically coupled nonlinear bistable vibration energy harvesting system, Figure 7(a) presents the stable equilibrium positions of beam 1 on the potential energy profile while Figure 7(b) shows the stable equilibrium positions on the potential energy profile of beam 2 using distance parameters L = 29.7mm, distance between magnets 1 and 3, and H = 21 mm, distance between magnets 1 and 2, and center offsets Δ_1 = 1.5 mm and Δ_2 = -1.6 mm. Note that the statically stable positons of the magnet centers shown are denoted as P_i and Q_i (i =1,2) respectively for beam 1 and beam 2. It refers that the tips of beam 1 and beam 2 remain on the i-axis and j-axis, respectively, when (i,j) = (0,0). The solid and dashed curves in Figure 7(b) are assessed when magnet 1 stays at stable equilibria P_1 and P_2, respectively.

The shape of the beam 1 potential energy profile in Figure 7(a) shows only one well in both solid and dashed lines. This indicates that beam 1 is monostable despite of the statically stable equilibrium where magnet 2 stays. The Figure 7(b), however, shows that beam 2 has the mirror symmetric double-well potential energy profiles in both solid and dashed lines which indicate that beam 2 has inherent bistable characteristics. Unlike the magnetically coupled single bistable energy harvester, this bistability in this energy harvesting system can be formed in asymmetric potential energy profile or transit to monostablility depending on the magnet spacing. This will be more clearly studied in later section for effect of magnet spacing. The benefit of the bistability is to dramatically improve energy conversion efficiency in the snap-through dynamic response when the beams are provided input energy. The dynamic characteristics are discussed in the later sections with various approaches. For this construction, when the tip of beam 2 rests on the equilibrium, Q_2, which is close to the magnet 1, it creates stronger magnetic force to magnet 1 and makes tip of beam stay on P_2. In the other case, when beam 2 in on positive side, Q_1, it generates less magnetic force since the tip of beam stay further from the j-axis as magnet 3 stays close to magnet 2. Thus, the potential energy profiles play a critical role to investigate the magnetic force and stable equilibria.

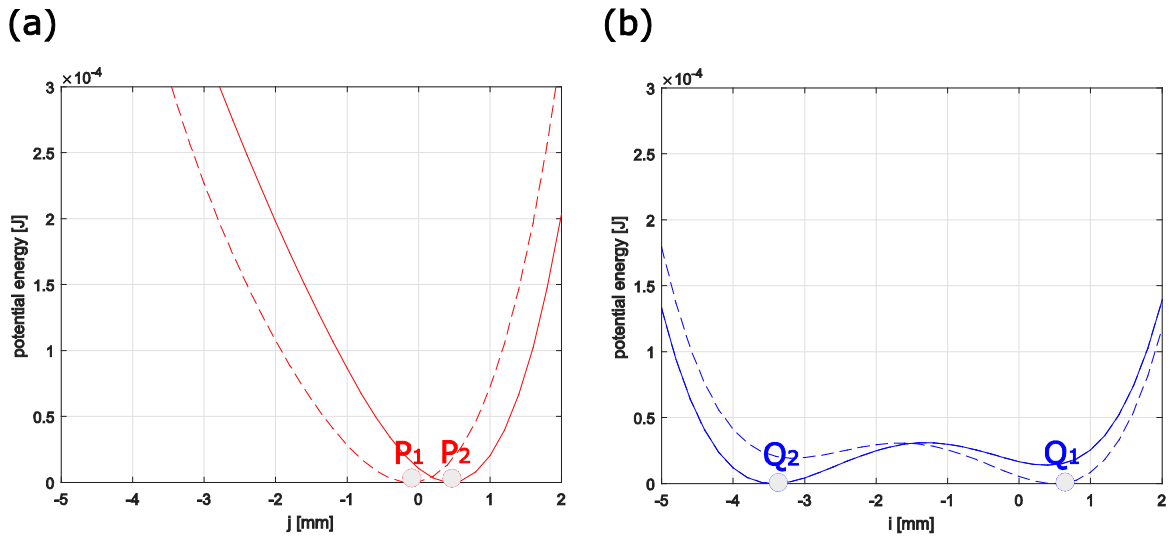

Figure 7. (a) Static stable equilibria (P_1, P_2) on the potential energy profile of beam 1 evaluated when beam 2 is fixed at static stable equilibria Q_1 and Q_2. (b) Static stable equilibria (Q_1, Q_2) on the potential energy profile of beam 2 evaluated

4.2 Validation of electrodynamic, nonlinear impulse responses

To verify the numerical approach to predict the dynamic response of the magnetically coupled nonlinear bistable energy harvesters, simulation and experiment results under impulsive excitations are compared. The quality of the impulsive excitations is translated as the initial velocity of the beam equivalent to the impulse energy applied to the beam. The coupled energy harvesting system is tested with the magnet offsets distances, Δ_1 = 1.5 mm and Δ_2 = -1.6 mm. For validation of simulation and experiment results match, Figure 8 shows that dynamic response results of experiment and simulation in different magnet distance L when an impulsive excitation is applied on beam 2 to the negative i-direction. In the experiment, impulsive excitation is applied on beam 2 at a stable equilibrium where beam 2 rests after previous dynamic response. The beam that is excited with impulse with short duration in experiment tends to be released at small distance from static equilibrium position where the beam rests previously. This kinetic energy is then converted to AC and DC voltages. Same amount of initial velocity measured in the experiment is applied in the simulation, and AC and DC voltages are converted from dynamic motion using governing equations shown in the previous section.

Figure 8(a), when L = 28 and H = 21 mm, shows the experiment result when beam 2 travels with initial velocity of 0.263 m/s. Beam 2 generate a DC voltage peak about 1.98 V while beam 1 generates a DC peak about 1.01 V by using the nonlinear magnetic forces delivered from beam 2. To compare this experiment result with electrodynamic response generated by simulation, same initial velocity and magnet distances values measured in the experiment are used as the initial input value. The simulation results shown in Figure 8(b) demonstrate that beam 2 generates maximum DC voltage about 1.88 V, and beam 1 generates about 1.02 V at the DC voltage peak. These close peak DC voltage values between experiment and simulation show a great agreement. In comparison of the AC voltage shape, both simulation and experiment have the similar shape with close frequency value. Those comparable trends between simulation and experiment are

also observed in the different magnet spacing construction as well. Overall, those similar trends lead to great agreement of validation between simulation and experiment.

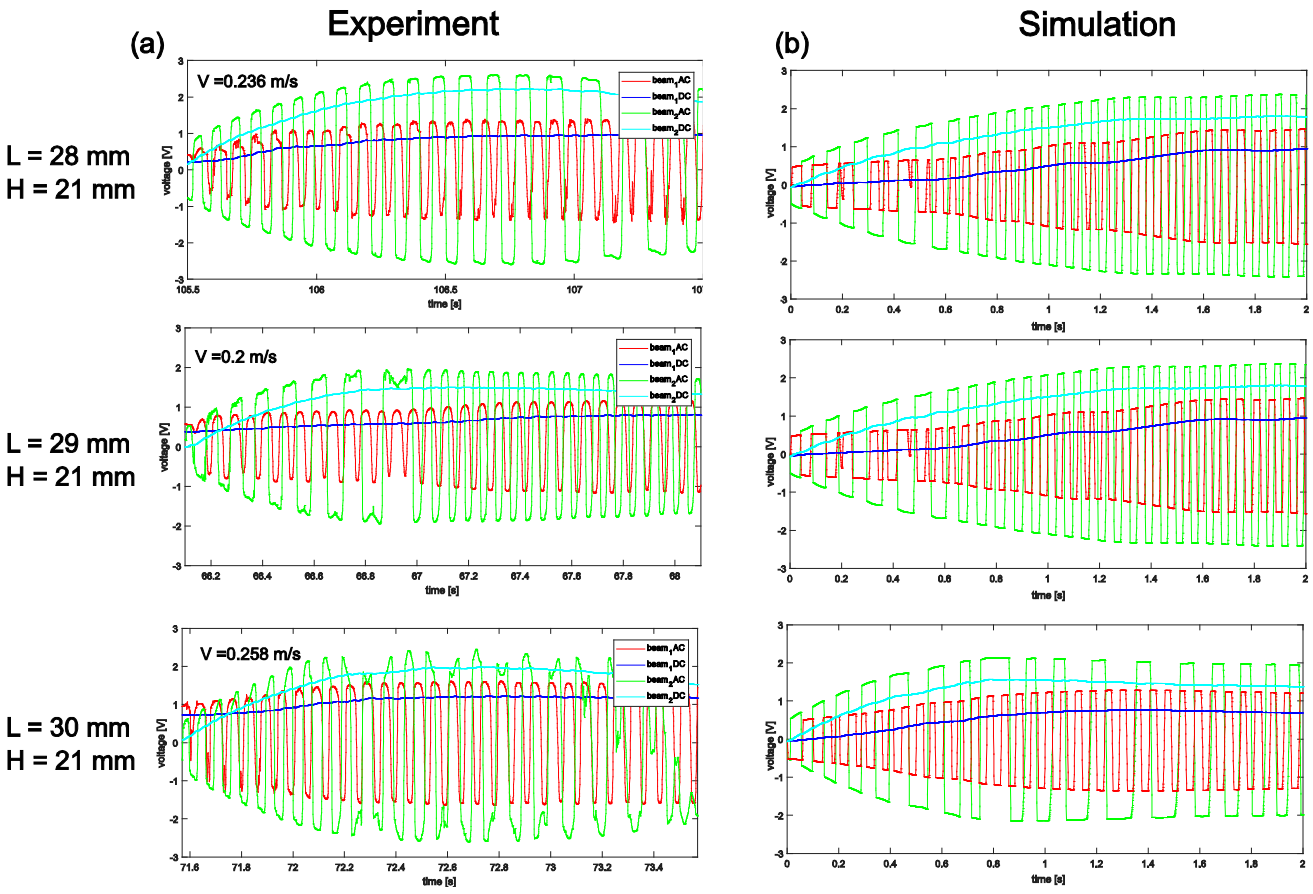

Figure 8. (a) Experimental AC and DC voltages for beam 1 and beam 2 (b) Corresponding simulation AC and DC voltages for beam 1 and beam 2

4.3 Examinations of magnet spacing in bistable energy harvester

The nonlinear vibration energy harvesters are strongly coupled by the repulsive magnets, and the nonlinear magnet forces are significantly influenced by the spacing between magnets. To understand the baseline of nonlinear magnetic forces, magnetically coupled single energy harvester beam is studied in this section prior to investigating the magnetically coupled double energy harvesting beam system. In a single nonlinear bistable vibration energy harvester beam, the fixed magnet is located on the same line as the beam is clamped, the distance between fixed magnet and moving magnet attached at the tip of the beam is only variable that changes the static magnetic forces. Figure 9(a) shows the potential energy profiles for the each magnet distance, Δ = 18, 19, 20 mm. . As the magnet spacing decreases, the shape of the potential files tend to create deeper potential wells while they sustain symmetricity. The potential energy at the barrier between two wells increase from 0.3 mJ to 1.2 mJ as distance, Δ, changes from 20 mm to 18 mm. The stronger magnetic force created by having smaller magnet distance make the right stable equilibrium move from 3.5

mm to 4.8mm. The left stable equilibrium also moves further from the center due to symmetricity of the sing beam energy harvesting system. Figure 9(b-d) show the total electrical energy generated by the single beam with assigned the magnet distance. As it is observed in the potential energy profile in the Figure 9(a), the single beam requires higher energy to travel from one static equilibrium to the other equilibrium as the magnet distance decreases. Thus, the harvester beam tends to have the snap-through vibration for shorter period of time followed by intrawell dynamic motion. The energy harvester also tends to generates inconsistent electrical energy output when the potential energy barrier between the stable equilibria becomes higher. These characteristics creates more scattered individual simulation data in Figure 9(b) than Figure 9(c) and (d). To obtain maximum energy from single energy harvester, tuning the magnet spacing may be considered as a key strategy.

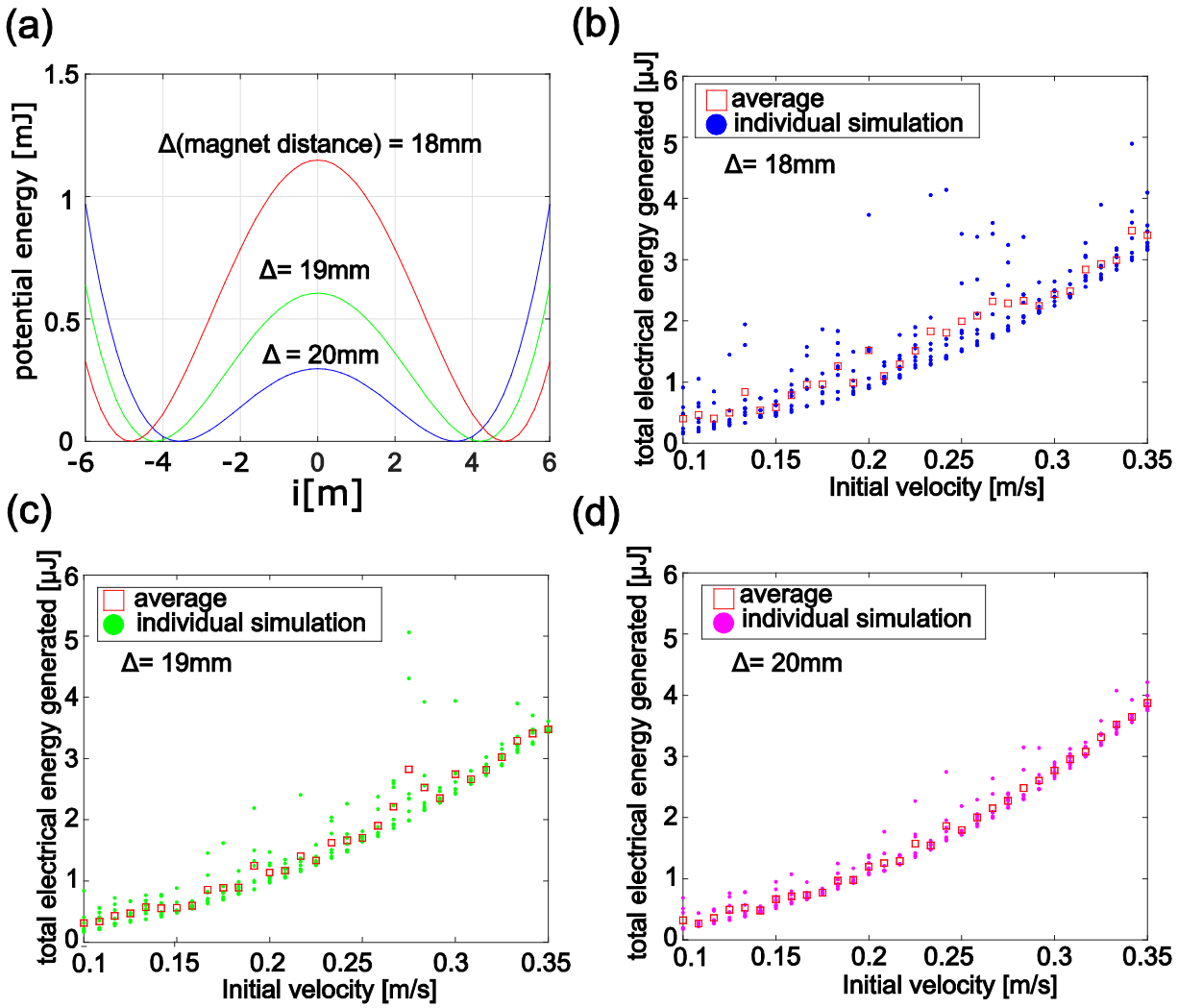

Figure 9 Single beam energy harvesting system (a) Potential energy profiles. (b) Total electrical energy generated at magnet distance, Δ = 18 mm. (c) Δ = 19 mm. (d) Δ = 20 mm.

The magnetically coupled nonlinear vibration energy harvesting system in this research inherently has more complexity due to the one fixed magnet and two moving magnets on the two harvester cantilever beams

oscillate in the different directions. The combination of the nonlinear magnetic forces tends to create both symmetry shown in Figure 10(b) and asymmetry potential energy profiles shown in the Figure 10(a,b). To understand more in influence of the magnetically coupled nonlinear energy harvesting system, changing distances L and H, and multi-directional impulsive excitations are conducted in both experiment and simulation. To comprehensively assess the dynamic response results, collected DC voltages output over time span are converted to total electrical energy generated by both beams 1 and 2. The total electrical energies are mainly influenced by the initial velocity applied on the beam.

Figure 10(d-f) show total electrical energies with corresponding initial velocity with different L distance and fixed distance H=21 mm, and Figure 10(a-c) show the potential energy profiles corresponding to configuration set as in Figure 10(d-f), simulation results, and Figure 10(g-i), experiment results. Individual data points in Figure 10(g-i) represent the single measurement of the integrated instantons DC power for 8 seconds once an impulse is applied to the beam. To satisfy the quantification of the experiment data quality, over 100 individual impulsive excitations were applied. The solid curve in Figure 10(g-i) demonstrate the moving average of single data points. Same as in the simulation shown in the Figure 10(d-f), the individual data points represent the single simulation of each run. The red colored squares are the average of the all the simulation points in the same initial velocity. The variance of the individual data points is generated by releasing points of the beam that is applied with impulse and the static equilibria for initial position. The potential energy profile, when L = 28 mm, in Figure 10(a) shows the asymmetry shaped potential energy wells where the static equilibrium at the right well has lower potential energy than the left one. In Figure 10(d), the averages of total electrical energies generated by the harvesting system with initial velocities 0.1 m/s and 0.35 m/s for beam 2 are 0.69 MJ and 4.53 MJ, respectively. The potential energy profile in Figure 10(b), when L= 29 mm, show symmetric shape of potential wells. The averages of total electrical energies at the velocities 0.1 m/s and 0.35 m/s for beam 2 are 0.22 MJ and 3.84 MJ, respectively as demonstrated in Figure 10(e).

The shape of the potential energy profile observed in Figure 10(c), when L= 30 mm, shows asymmetry like the potential energy profile shown in Figure 10 (a), but opposite mirror appearance, which the static equilibrium in the left well has lower potential energy. The averages of total electrical energies at the velocities 0.1 m/s and 0.35 m/s for beam 2 are 0.44 μJ and 4.14 μJ as shown in Figure 10(f). In comparison between symmetric and asymmetric potential energy profiles, the averages of total electrical energy generated in the system tend to be greater with asymmetric potential energy profile than symmetric potential energy profile. The potential energy is related with the amount of force required to move the mass against resistant forces acting on the beam. Thus, it requires more force to deliver beam from one static equilibrium to the other as the potential energy between the two potential well increases. In the case of asymmetric potential energy profile, the distance that the beam travels, when same amount of impulsive excitation was applied to the beam, varies depending on the initial resting position. This explains why individual data points are more scattered in Figure 10(d,f) which have the asymmetric potential energy profile than ones in symmetric potential energy profile in Figure 10(e).

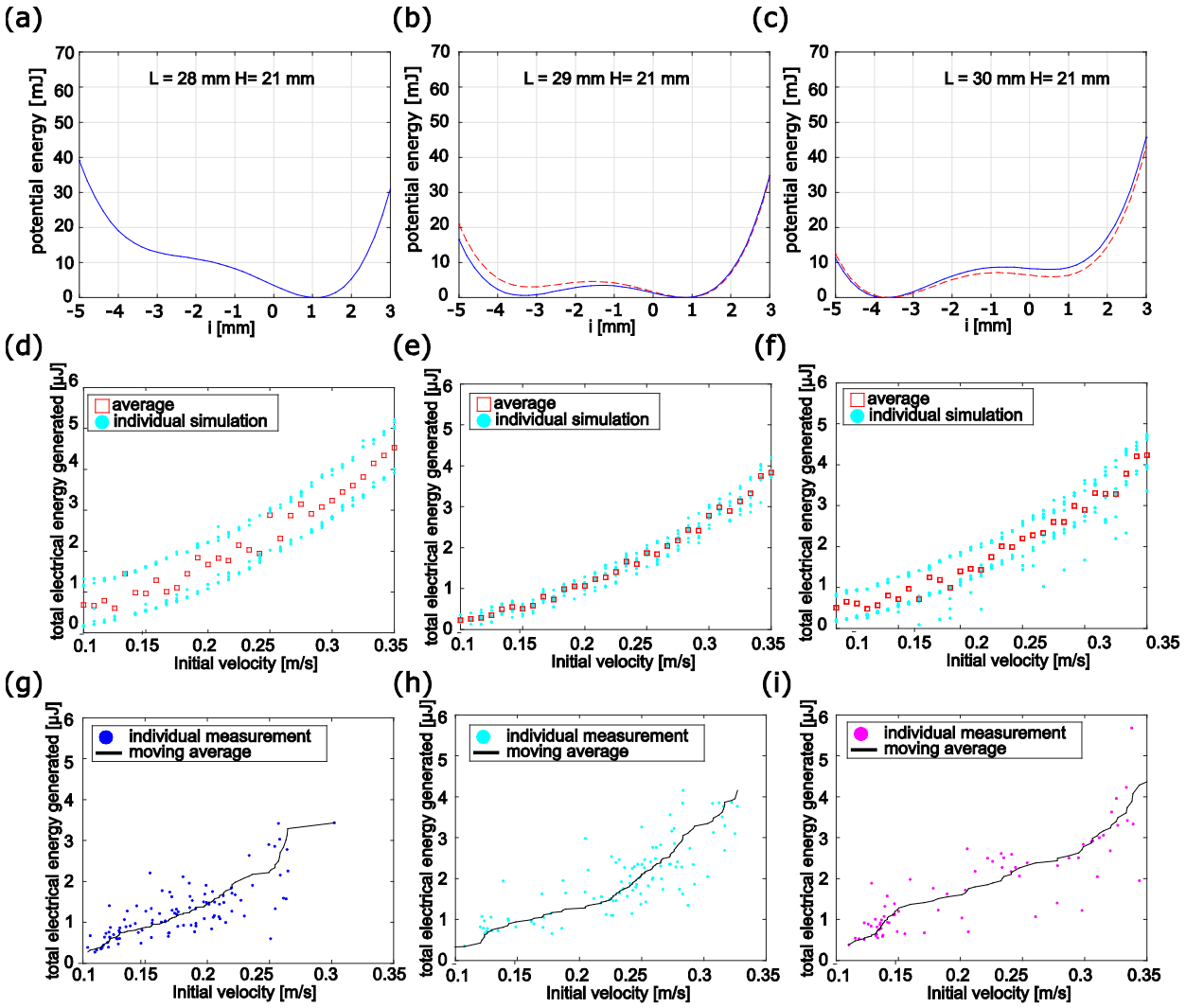

Figure 10. Impact of magnet distance, L. (a-c) Potential energy profile at L = 28, 29, and 30, respectively with fixed distance H at 21mm. (d-f) Simulation: total electrical energy generated. (g-i) Experiment: total electrical energy generated. The plots at each column are generated with same magnet distances.

To observe characteristics caused by varying distance H by moving magnet 3 along the j-axis, the distance L is fixed in 28 mm from the j-axis, and beam 2 is impulsively excited to the negative i-direction. Figure 11(a) demonstrates the potential energy profile, when H = 20 mm, which clearly shows double potential energy well. Figure 11(d) shows corresponding total electrical energy generated along with initial velocity assigned as input energy. In this L and H setting, the individual data plots are less scattered until the initial velocity is 0.15 m/s and begins to diverge into the two main trend lines. The concentrated data points at the low initial velocities is caused since it has slightly lacking symmetric potential energy profile which require almost same energy input for beam to overcome the hill between the two wells. The potential energy differences between stable equilibrium and the middle peak have minimum of 8 mJ and maximum of 12 mJ depending on the stable equilibrium that beam 2 rests while Figure 11(a,b) show significantly low potential energy differences or monostable equilibrium. Thus, the beam 2 tends to have interwell

oscillations when the impulsive excitation energy is less than the potential energy of the hill while beam 2 can have snap-through vibration when the beam 2 initially dwells in the higher stable equilibrium like left well of dashed line in Figure 11(a). When the enough impulsive energy is delivered to the beam, the beam 2 begins snapthrough oscillations and obtain different amount of electrical energy depending on the initial displacement of the magnets. Figure 11(b) shows the left potential energy well rises as magnet 3 is located further from the magnet 2. The less force from magnet 3 brings the right stable equilibrium from 1.5 mm to 1.3 mm as the magnet distance, H, changes from 20 mm to 21 mm. This asymmetric shape potential energy profile results have the two separate trend lines with the individual total electrical energy data points in the Figure 11(e). As it is observed in the results by changing magnet distance, L, the averages of the total electrical energy generated with asymmetric potential energy profile at each initial velocity tend to be greater than ones with the symmetric potential energy profile. The Figure 11(c) shows the single well potential energy profile when H = 22mm. The less magnetic field of magnet 3 is in contact with magnet 2's magnetic field, the weaker magnetic force to push beam 2 to negative i-axis is created. This weak force delivered from the magnet 3 is then overwhelmed by the force from magnet 1, and the beam 2 eventually has only single static equilibrium. The monostable potential energy profile results in the only one trend line of concentrated individual data points. In comparison with the average of total electrical energy generated by bistable setting, the average of total electrical energy generated by the monostable setting are observed to be low by about 1 μJ in general.

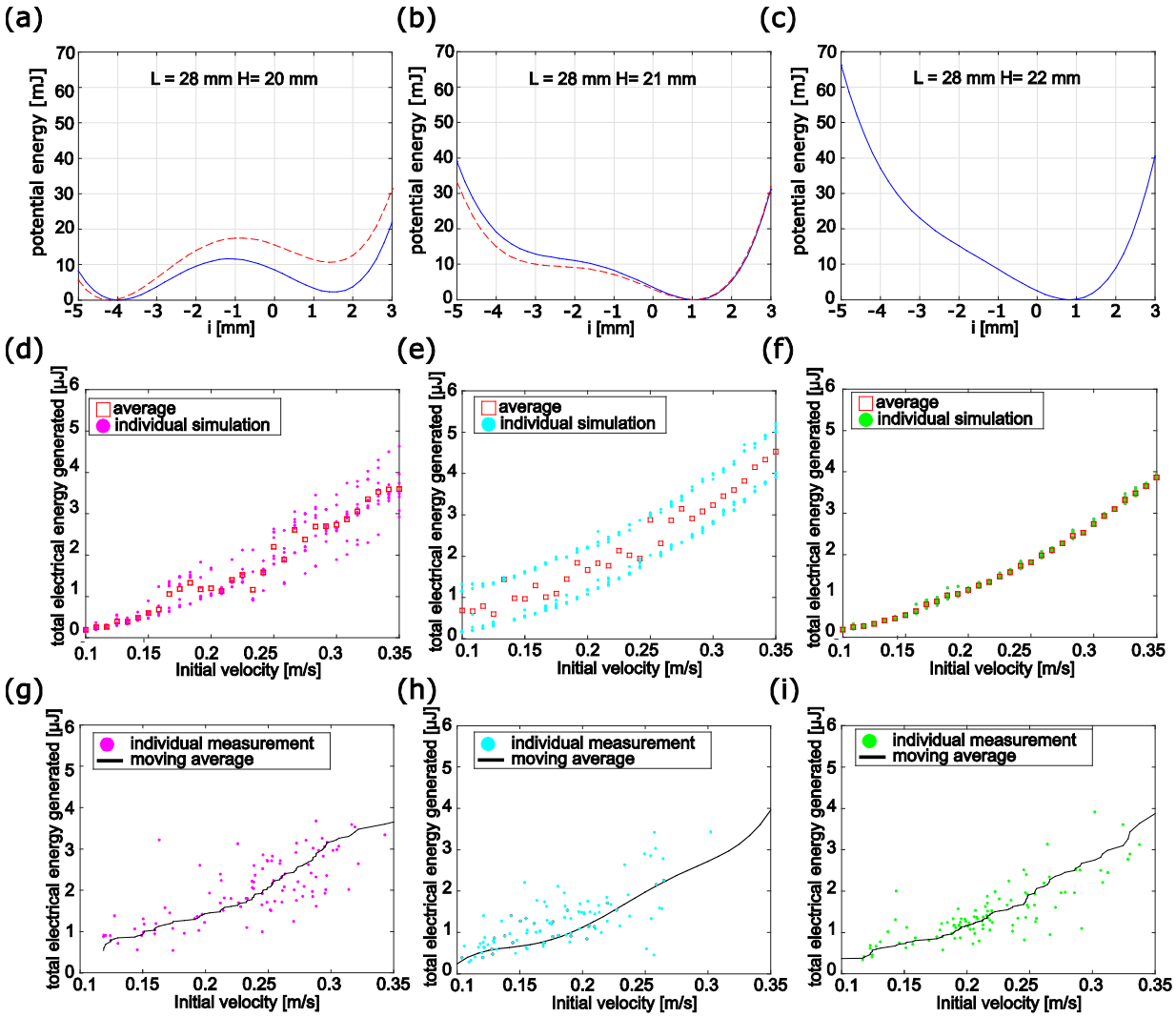

Figure 11. Impact of magnet distance, H. (a-c) Potential energy profile at H = 20, 21, and 22, respectively with fixed distance L at 28mm. (d-f) Simulation: total electrical energy generated. (g-i) Experiment: total electrical energy generated. The plots at each column are generated with same magnet distances.

Based on the characteristics of the nonlinear vibration energy harvester, the total electrical energy generated by both beams 1 and 2 show parabolic concavity trend as the initial velocity increases in both simulation and the experiment results. Despite of the limitations and conditions related with the experiments, the overall trends are generally matched between simulation and experiment. These total electrical energy results along with the wide range of initial velocities enhance the validation between experiment and simulation.

4.4 Examination of magnet center offset in bistable energy harvester

Based on the results by changing magnet spacing in the magnetically coupled energy harvesting system, the magnet displacements have great influences on the static equilibria of beams and the magnetic forces. In addition to changing distances between magnets, adjusting the center offset distance of magnet 2 can generate different electrical energy. Figure 12 shows total electrical energy converted at the three different

center offset distance of magnet 2 with the constant initial velocity of 0.2 m/s. The Figure 12(a-c) are generated with magnet 2 offset distances, Δ_2=-1.4, -1.6, and -1.8 mm on i-axis, respectively as the L distance increases, and the H distance is fixed in 21mm. The characteristic in Figure 12(a) shows that the individual simulation points tend to diverged and form two trend lines. The two lines are formed symmetry about the point where the lines merge into. These two different energy trend lines are created through the bistable characteristics of the magnetically coupled energy harvesters. To more clearly explain this, Figure 13 shows two different dynamic motion and electrical power with the asymmetric potential energy profile. When the harvester beam 2 is initially excited at stable equilibrium, Q_2, beam 2 has less snap-through dynamic motion and generate less current in both beam 1 and beam 2, as shown in Figure 13(b,d), than when beam 2 initially is excited at the static equilibrium at stable equilibrium, Q_1 as depicted in Figure 13(c,e). The overall trend shown in Figure 12(a) also appears in Figure 12(b,c), but the data points are shifted to the left as the center offset distance increases due to the different responding magnet forces.

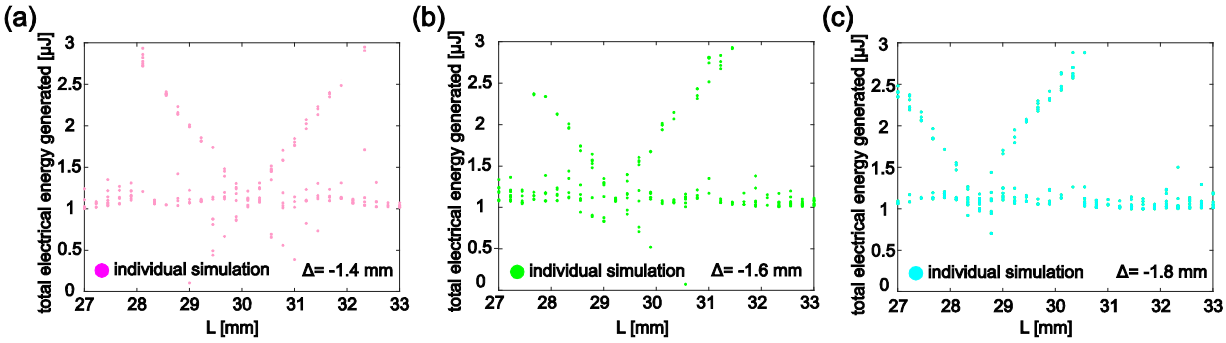

Figure 12. Total electrical energy generated depending on the magnet distance L potential energy profiles (a) Δ_2 = -1.4 mm. (b) Δ_2 = -1.6 mm. (c) Δ_2 = -1.8 mm

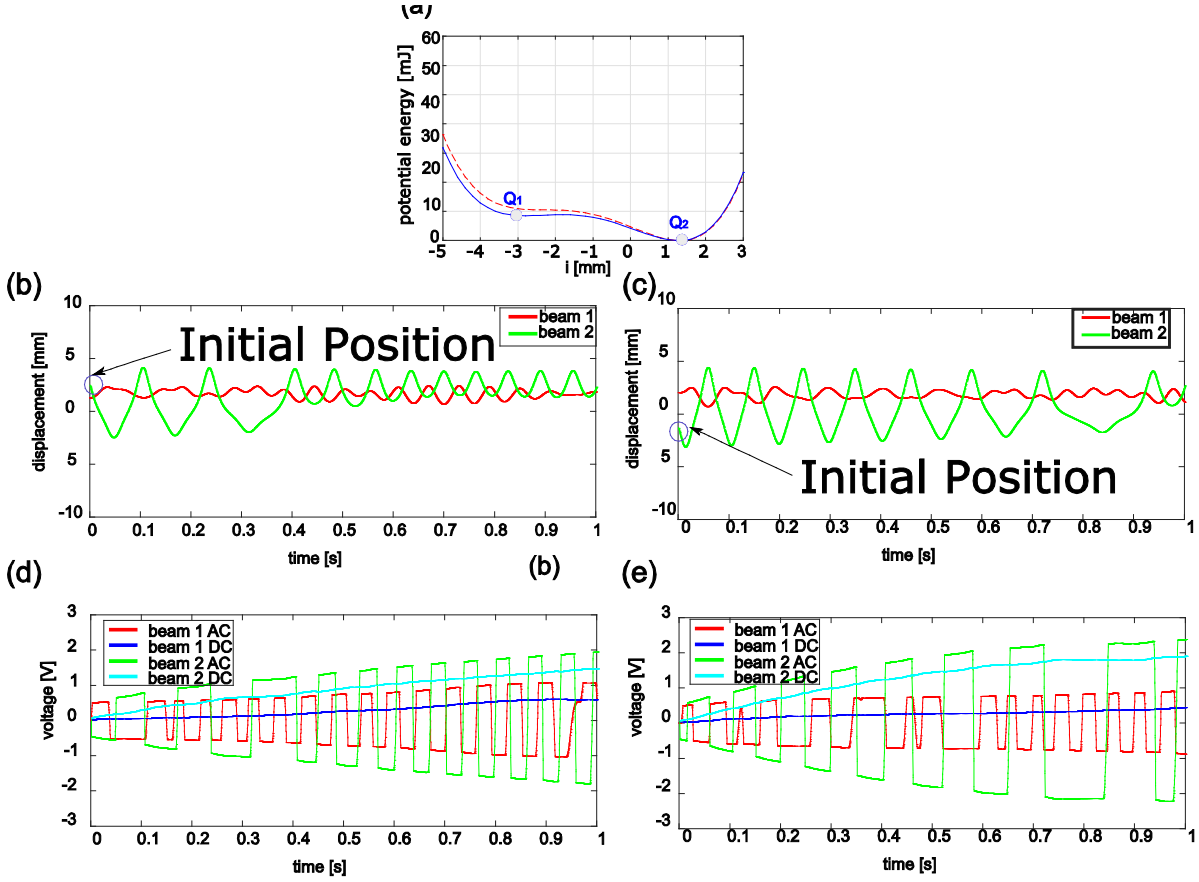

Figure 13. At Δ_2 = -1.4 mm, L = 29mm, and H = 21 mm. (a) potential energy profile. (b,d) Dynamic response with initial location at stable equilibrium Q_2 and Q_1, respectively. (c,d) AC and DC power generated in each beam with initial location at stable equilibrium Q_2 and Q_1, respectively

To compare relationship more detail, Figure 14(a-c) shows the potential energy profiles of beam 2 in three different offset setting with fixed distances L=30 and H=21. Beam 1 has mono-stability with one well in the potential energy profile regardless of the magnet distances as it was studied in the section 4.1. Thus, the shapes of potential energy profiles of beam 1 are not greatly influenced by varying the small center offset distance. Beam 2 in this distance setting, however, form different shapes of potential energy profiles with the bistable characteristics. Figure 14(a) shows two equilibria are at P_1=-3.4 mm and P_2=1.2 mm with potential energy 0 and 2.331 μJ, which the shape of the profile looks symmetric. Figure 14(b) reveals that the two potential wells are at Q_1= -3.6 mm and Q_2= 0.6 mm with potential energy 0 and 59.17 μJ, respectively. This indicates the right potential well rises when the offset value increases in comparison between Δ_2= -1.4 mm and Δ_2= -1.6 mm. Figure 14(c) shows the R_1= -4 mm and R_1= 0.4 mm with 0 and 128.6 μJ. As comparison between Δ_2= -1.4 mm and Δ_2= -1.6 mm, the right potential well rises more with Δ_2= -1.8 mm than Δ_2= -1.6 mm. This makes the right side of the potential profile of Δ_2= -1.6 mm seem close to a horizontally flat line than a well. These series of results shows the different center offset of the magnet 2 can form both symmetric to asymmetric potential energy profile shapes. The different level of potential energy between two static equilibria induces beam 2 to rest at the lower stable equilibrium more frequently

after its dynamic motions. For example, the tip of beam 2 in asymmetric potential profile as in Figure 14(b) may more repeatedly rest at the left potential well which has lower potential energy [32].

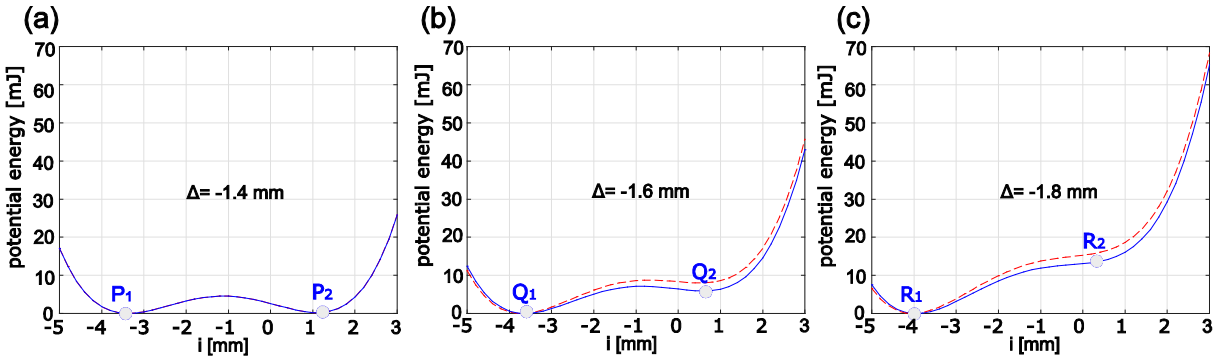

Figure 14. Potential energy profiles of harvester beam 2 at L = 30mm and H =21mm with magnet center offset distance between magnets 2 and 3. (a) Δ_2 = -1.4mm. (b) Δ_2 = -1.6 mm (c) Δ_2 = -1.8 mm

Using the same center offset parameter, and same distances L and H setting values, the dynamic responses of the magnetically coupled nonlinear energy harvester is investigated utilizing compatible simulation model. Figure 15 shows the result of the beam tip displacement and the converted electrical power in 1 second after beam 2 was impulsively excited. Figure 15(a) with Δ_2= -1.4 mm shows the snap-through dynamic motions of beam 2 for about 6.3 seconds, and the maximum DC voltages generated by the beams 1 and 2 are 0.997 V and 1.437 V, respectively. Figure 15(b) Δ_2= -1.6 mm shows snap-through dynamic motion of beam 2 for about 4.7 seconds, but less number of pass between wells than the vibration with Δ_2= -1.4 mm. The maximum DC voltages generated by beams 1 and 2 are 1.026 V and 1.083 V, respectively, which shows less electrical power generated by beam 2 in comparison with the power generated with Δ_2= -1.4. In Figure 15(c) shows only intrawell dynamic motion of beam 2 which refers beam 2 oscillates around same stable equilibria where the beam initially begins its vibration. The dynamic motions of the beams result in the maximum DC voltages of the beams 1 and 2 to be 1.287V and 0.8233 V, respectively. The small amplitude of the vibration in beam 2 is converted to the smaller maximum DC power. Overall, the maximum DC power generated by beam 2 decreases as the center offset distance increases while the maximum DC power generated by beam 1 increases. As it is observed in Figure 14, beam 2 in asymmetric potential energy profile tends to rest in the equilibrium on the negative i-axis, which has the lower potential energy when multiple simulation was performed. Thus, understanding the role of offset distance is also important key along with distance L and H for the strategy to get maximum electrical energy in the magnetically coupled nonlinear energy harvesting system.

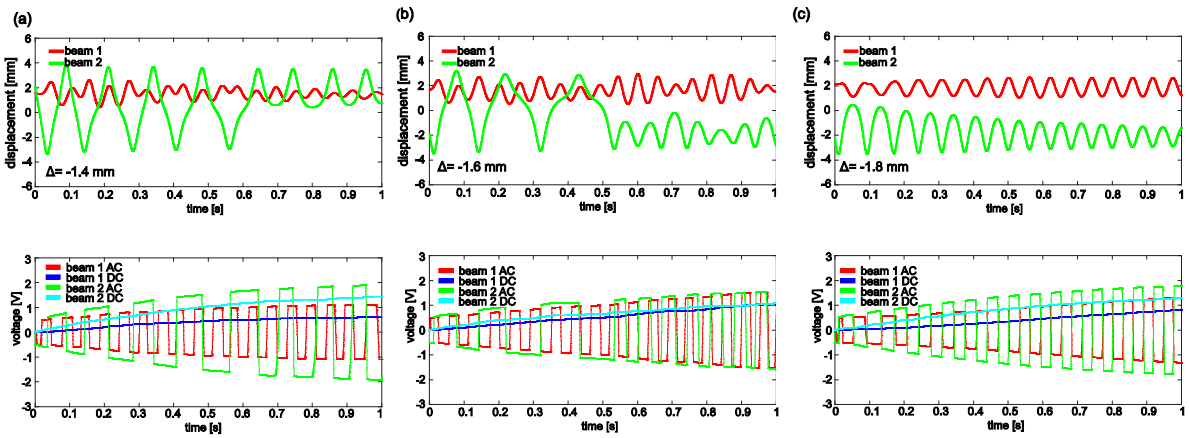

Figure 15. The behavior of beams 1 and 2, and AC and DC electrical power in dynamic response when beam 2 is perturbed from the stable equilibrium closer to beam 1 with initial velocity 0.2 m/s of (a) Δ_2 = -1.4 mm. (b) Δ_2 = -1.6 mm. (c) Δ_2 = -1.8 mm.

4.5 Evaluation of energy conversion with multi-directional impulsive excitation

Based on the results obtained through different magnet distance setting and initial velocity perturbation, the potential energy profiles and total electrical energy generated by the entire energy harvesting system have been observed in the previous section. In this section, the symmetry and asymmetry of the energy harvesting system will be compared and contrasted in detailed with energy conversion performed by beams 1 and 2 separately. In addition, multi-directional impulsive excitations are investigated to consider more situation involved with the energy harvester. Figure 16 shows the average electrical energy converted for individual simulation data points by each harvester beam at the assigned initial velocity perturbation. The portion of electrical energy converted by beam 1 in the bars are covered with yellow color while the blue color in the bars represent the portion of electrical energy converted by beam 2. The height of the bars represent the total electrical energy generated by the entire system. To compare the energy conversion more strictly, the electrical energy converted by a single nonlinear bistable energy harvesting system is laid on the same plots as benchmark. The magnet spacing for the single energy harvester is set to be 21 mm, which is the optimized system configuration that generates the maximum energy in the system. The benchmark energy conversion is shown as red square makers connected by solid line.

Figure 16 demonstrates the energy conversion at the different distance L with fixed H = 21 mm. The distance L values are selected to generate a perfect symmetric and two mirrored asymmetric potential energy profile shape. Figure 16(a-c) show the potential energy profile for each magnet distance setting. The following plots in the same column use the same magnet distance setting as which the potential energy profiles use in the first low. The second row, Figure 16(d-f), represent the energy conversion result when beam 2 is impulsively excited to negative i-direction. The third row, Figure 16(g-i), refers the energy conversion results when beam 1 is impulsive excited to negative j-direction while the fourth row, Figure 16(j-l), refers results when both beams are excited spontaneously with same amount of impulsive energy. In comparison of energy conversion when beam 2 is initially excited, the total electrical energies generated

by the entire energy harvesting system with asymmetric potential energy profiles in Figure 16(e,d) are generally greater than the benchmark while the total electrical energies generated by the system with symmetrical potential energy profile are lower at the most initial velocity perturbation. In terms of the portions that each beam generates, the dark blue shade in the bars, energy generated by beam 2, tends to occupy more portion in the bars than the yellow shade. In addition, the portion of the bars occupied by the blue shade tends to increase as the initial velocity increases while the portion of the bars occupied by the yellow shade are not observed to have great changes, but rather gradually increases. In comparison of energy conversion when beam 1 is impulsively excited in Figure 16(g-i), the energy conversion performed by beam 1 occupies great portion in the bars at all the initial velocities used. The harvester setting with asymmetric potential energy profiles in Figure 16(g) tend to have more energy generated by beam 2 than one with symmetric potential energy profile in Figure 16(h) at all initial velocities. The energy generated by beam 2 in Figure 16(f), however, tends to be greater than energy generated by beam2 in Figure 16(e) only at the velocities above 2.5 m/s. This characteristics can be explained with the asymmetry in Figure 16(c) which has lower potential energy in the left stable equilibrium than the right stable equilibrium. This requires more energy input for tip of beam 2 to travel from the left well to the right well. Thus, beam 2 starts to have snap through oscillations when higher force from magnet 1 is delivered to magnet 2. As the characteristics of the energy harvesting system under impulsive excitation on single beam is studied, combined characteristics of two cases, 1) beam 1 is excited, 2) beam 2 is excited, appears when the both beams are excited. The total electrical energy generated by the system is significantly greater than the benchmark regardless of the distance L set for the system.

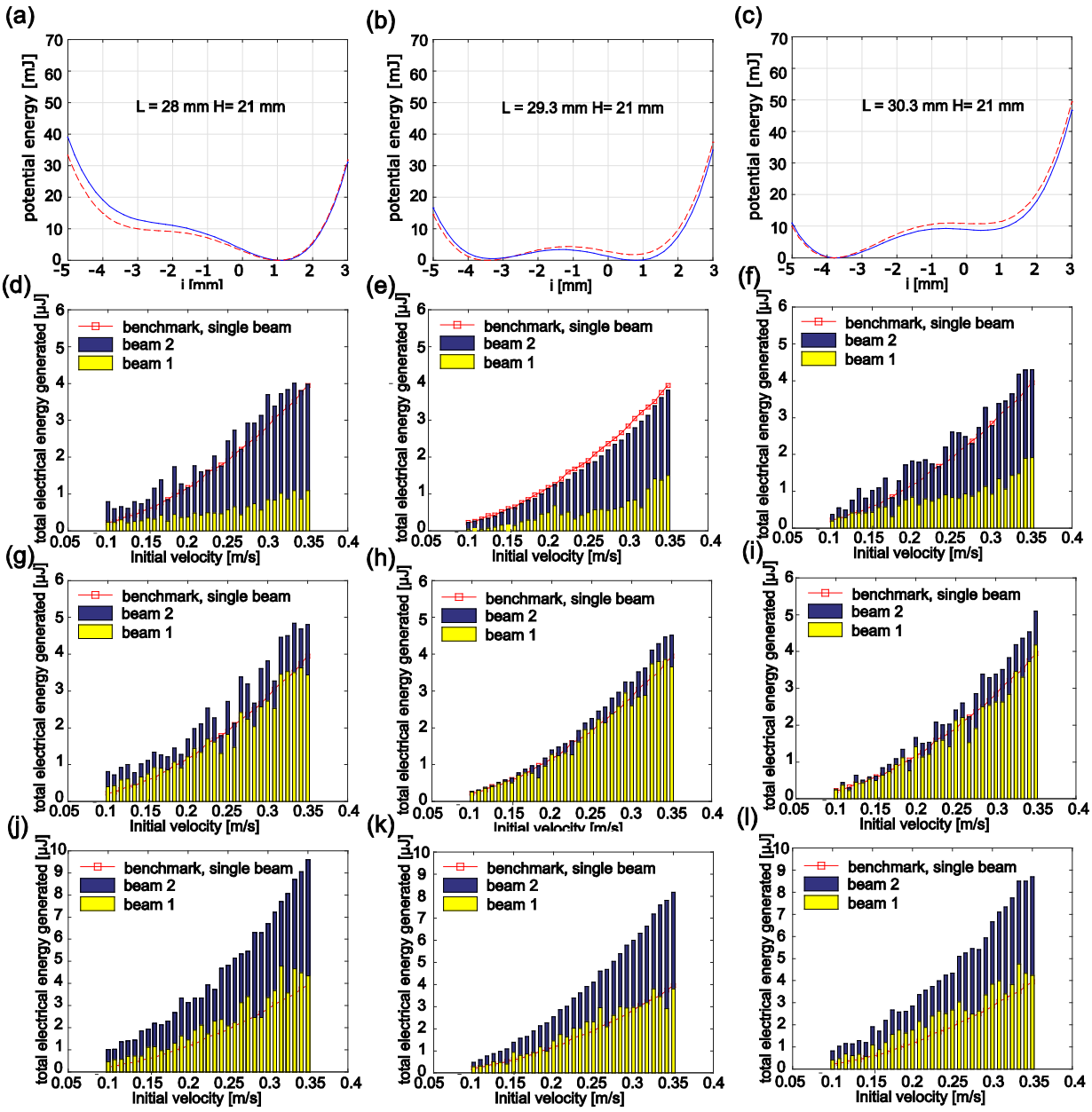

Figure 16. Comparison of energy conversion in symmetry vs asymmetry changing distance L. (a-c) Potential energy profile at L = 28 mm, L = 29.3 mm, and L = 30.3 mm with fixed H = 21 mm, respectively. (d-f) Impulse on beam 2. (g-i) impulse on beam 1. (j-l) impulse on both beam at the same time. The figures in the same column correspond with the potential energy profiles in the first row.

The Figure 17 demonstrates the energy conversion with change of H and fixed L= 28.3 mm. The array of the plots in the Figure 17 is same as Figure 16. Figure 17(a), when H= 20mm, shows the high potential energy hill between the two static equilibria while Figure 17(b) shows symmetry in the shape with low potential energy hill between the static equilibria. With the asymmetry in potential energy profile, it shows again that the energy generated by the each beam in Figure 17(d) is much greater than the ones in Figure 17(e). Figure 17(c), when H= 22 mm, shows that the harvester system create mono-stable equilibrium due

to less magnetic force from magnet 3. The potential energy, however, gradually increases before it suddenly increases around -3 mm on the i-axis, and the potential energy before the steep slope is still greater than the highest potential energy peak in between the static equilibria in Figure 17(b). This results in which the total electrical energy generated in Figure 17(f) is greater than the total energy generated in Figure 17(e). The electrical energy generated by beam 2 in Figure 17(e) is, however, greater than in Figure 17(f). In comparison of the total electrical energy generated under impulsive excitation on beam 1, Figure 17(i) has greater amount of total energy generated comparing with benchmark while Figure 17(g,h) do not show exceeding total electrical energy until the initial velocity is 0.2 m/s. In the case of double potential wells, the beam 2 resting in further stable equilibrium from magnet 1 is not greatly affected by the magnetic force by magnet 1 when the beam 1 is impulsively excited. On the other hand, in the case of monostable configuration shown in Figure 17(c), the stable equilibrium is located relatively closer to the magnet 1, where there is more magnetic force from magnet 1. In addition, the gentle slope on the negative i-axis of the potential energy profile helps beam 2 have wide amplitude oscillation. These characteristics of monostability in the energy harvesting system have higher energy generation when beam 1 is impulsively excited with low initial velocities. Figure 17(j-l) under impulsive excitation on the both beams show excellently great total energy generated compared to the benchmark. The insight here is that the energy generated only by the beam 1 in Figure 17(j) greatly increased from Figure 17(g), which only beam 1 is applied with impulsive excitation, while the electrical energy generated by beam1 in Figure 17(k,l) are not found to be great improvement from Figure 17(h ,i), respectively.

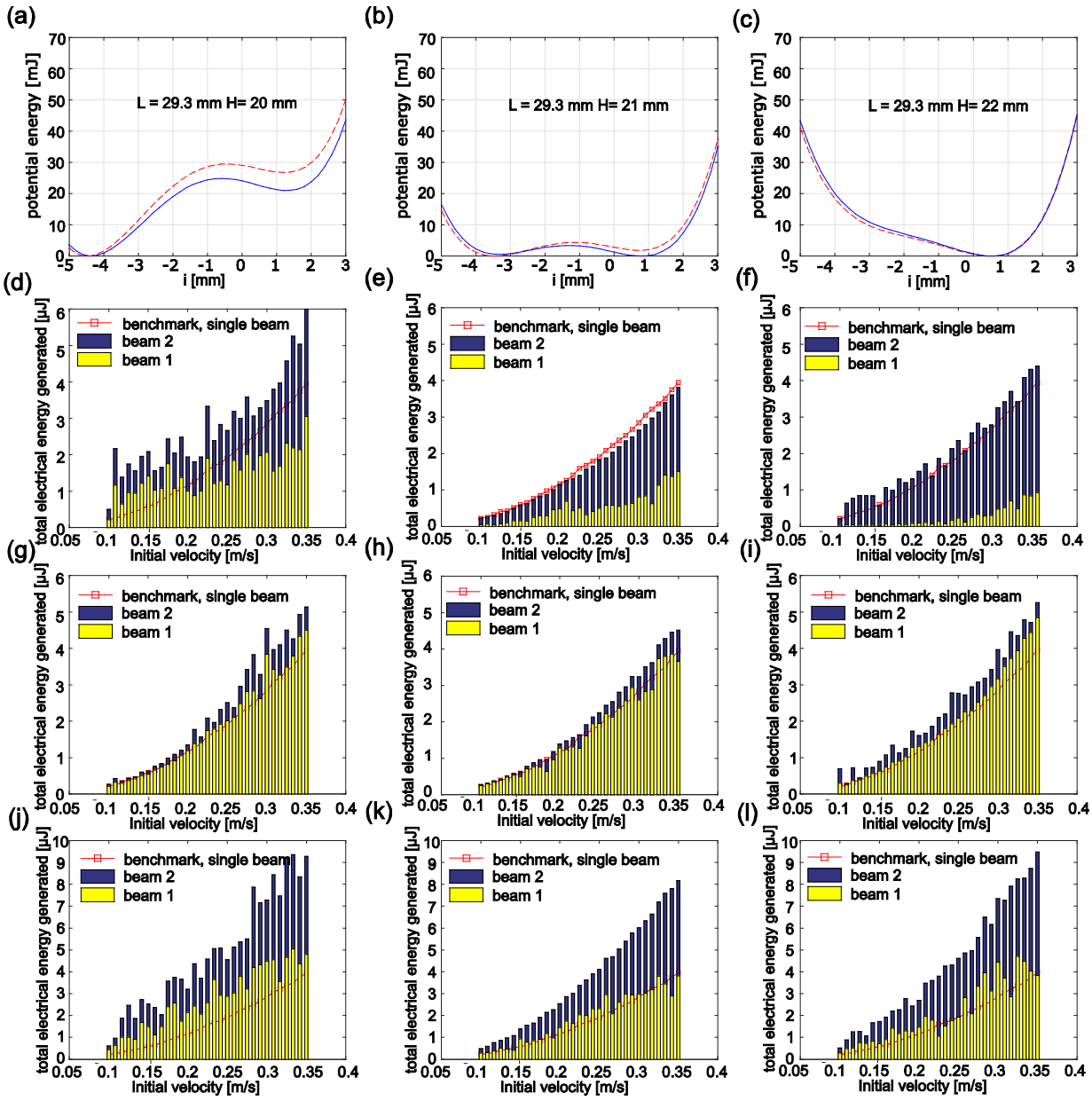

Figure 17. Comparison of energy conversion in symmetry vs asymmetry changing distance H. (a-c) Potential energy profile at H = 20 mm, H = 21 mm, and H = 22 mm with fixed L = 29.3 mm, respectively. (d-f) Impulse on beam 2. (g-i) impulse on beam 1. (j-l) impulse on both beam at the

Based on the equation (2), the load resistance, R, act as an important role as consideration of electric energy quality. To generate the maximum electrical energy output, finding optimum DC load resistance is important. Figure 17(a) shows the electrical energy generated by each beam across the DC load resistance with range between 1 MΩ to 1 GΩ. The maximum electrical energies occur at the resistance value of around 20 MΩ for both beams 1 and 2. Figure 17(b,c) in different configuration set up also demonstrate the electrical energy along the DC load resistances. The three plots with different configurations in Figure 18

prove that the maximum electrical energy are generated with the same DC load resistance regardless the different magnet distance in the energy harvesting system setup.

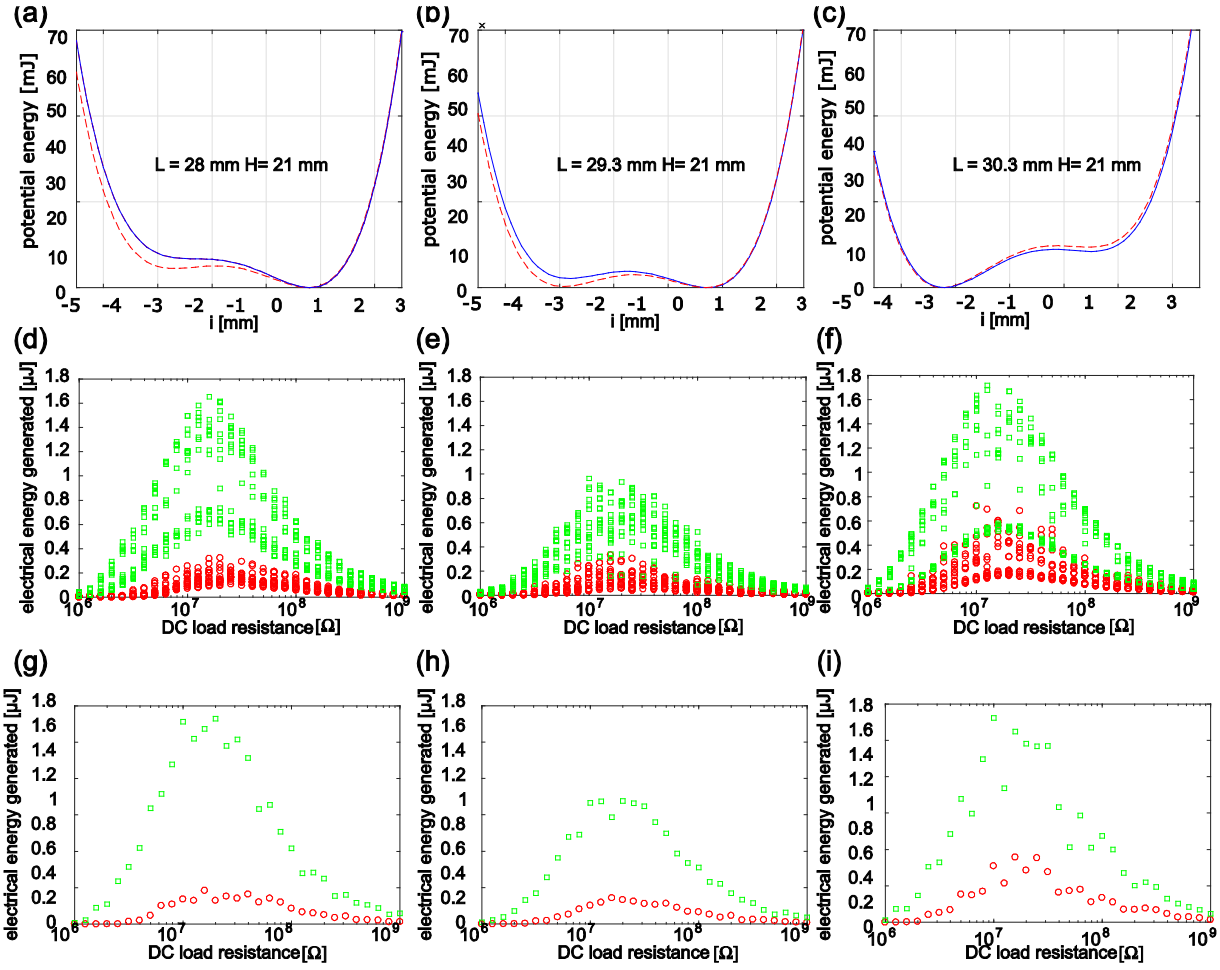

Figure 18. Electrical energy generated by each beam when beam 2 is perturbed with initial velocity 0.2 m/s Resistance sweep (a-b) Potential energy profile (d-e) with L = 28 mm, L= 29.3 mm, and L = 30.3 mm with fixed H = 21 mm. (b) energy energrated in each beam depending on load resistance. (g-i) average of individual energy generated along each load resisance

5 Conclusion

Impulsive vibration is popular ambient vibration form that exist in various structures and human motion. Harnessing this allowed ambient energy source in the environment is a great opportunity for energy conversion. Previously, the nonlinear bistable vibration energy harvesters are proved to have great performance under impulsive excitation. To the date, there is still gap of knowledge in magnetic forces in the magnetically coupled nonlinear vibration energy harvesting system in despite of the many previous efforts.

Using the magnetically coupled nonlinear bistable vibration energy harvester, this research both analytically and experimentally investigate to characterize the nonlinear coupling and energy conversion properties. The static equilibria and the dynamic response subjected to impulsive excitation are investigated to find the strategy for maximizing capturing kinetic energy and energy conversion. The results of this research bridges the gap of knowledge on nonlinear multi-directional magnetic forces.

As it is observed utilizing compatible numerical model over broad range of configuration variable, the energy generated by the energy harvesting system is significantly depending on the magnet spacing. Manipulating the magnet spacing provides both symmetric and asymmetric potential energy profiles regarding the potential energy at the static equilibria. The investigation proves that the asymmetry in the potential energy profile tend to generate superior total electrical energy to the symmetric one.

These two cases are also investigated under situation where impulsive excitation is applied on different beam using numerically compatible model. The results from this investigation also prove that magnet configuration with asymmetry of potential energy profile tends to generate more energy than the configuration with symmetry of potential energy profile. Lastly, the investigation on the DC load resistance as variable for energy conversion prove that the maximum total electrical energy occurs at the same optimum DC load resistance regardless of the magnet configurations.

The results of this research provide fundamental knowledge for the magnetic coupling effect in the nonlinear vibration energy harvester. Future work will involve numerical simulation of impulsive energy qualities like change of duration and periodicity in order to observe the characteristics of magnetically coupled energy harvesters and how energy conversion varied depending on the quality of the impulsive excitation. Characterizing the nonlinear vibration energy harvesters will provide a good understands on the real-time application subjected to random ambient impulsive excitations.

REFERENCES

[1] R. Randall, Vibration-based Condition Monitoring: Industrial, Aerospace and Automotive Applications, Chichester: Wiley, 2011.

[2] P. Green, E. Papatheou and N. Sims, "Energy harvesting from human motion and bridge vibrations: an evaluation of current nonlinear energy harvesting solutions," *Journal of Intelligent Material Systems and Structures,* vol. 24, pp. 1494-1505, 2013.

[3] S. Beeby, M. Tudor and N. White, "Energy harvesting vibration sources for microsystems applications," *Measurement Science and Technology,* vol. 17, pp. R175-R195, 2006.

[4] S. Roundy, "On the effectiveness of vibration-based energy harvesting," *Journal of Intelligent Material Systems and Structures,* vol. 16, pp. 809-823, 2005.

[5] E. Yeatman, "Energy harvesting from motion using rotating and gyroscopic proof masses," *Proceedings of the Institution of Mechanical Engineers, Part C: Journal of Mechanical Engineering Science,* vol. 222, pp. 27-36, 2008.

[6] M. Daqaq, "Transduction of a bistable inductive generator driven by white and exponentially correlated Gaussian noise," *Journal of Sound and Vibration,* vol. 330, pp. 2554-2564, 2011.

[7] M. Daqaq, "Response of uni-modal duffing-type harvesters to random forced excitations," *Journal of Sound and Vibration,* vol. 329, pp. 3621-3631, 2010.

[8] S. Stanton, B. Mann and B. Owens, "Melnikov theoretic methods for characterizing the dynamics of a bistable piezoelectric inertial generator in complex spectral environments," *Physica D,* vol. 241, pp. 711-720, 2012.

[9] K. Ylli, D. Hoffmann, A. Willmann, P. Becker, B. Folkmer and Y. Manoli, "Energy harvesting from human motion: exploiting swing and shock excitations," *Smart Materials and Structures,* vol. 24, p. 025029, 2015.

[10] K. Suhaimi, R. Ramlan and A. Putra, "A combined softening and hardening mechanism for low frequency human motion energy harvesting application," *Advances in Acoustics and Vibration,* p. 217032, 2014.

[11] M. Karami and D. Inman, "Controlled buckling of piezoelectric beams for direct energy harvesting from passing vehicles," in *Proceedings of the ASME 2012 International Design Engineering*

Technical Conferences and Computers and Information in Engineering Conference, Chicago, IL, USA, 2012.

[12] A. Stacoff, C. Diezi, G. Luder, E. Stüssi and I. Kramers-de Quervain, "Ground reaction forces on stairs: effects of stair inclination and age," *Gait and Posture,* vol. 21, pp. 24-38, 2005.

[13] R. Harne and K. Wang, "A review of the recent research on vibration energy harvesting via bistable systems," *Smart Materials and Structures,* vol. 22, p. 023001, 2013.

[14] B. Mann and N. Sims, "Energy harvesting from the nonlinear oscillations of magnetic levitation," *Journal of Sound and Vibration,* vol. 319, pp. 515-530, 2009.

[15] L. Gu and C. Livermore, "Impact-driven, frequency up-converting coupled vibration energy harvesting device for low frequency operation," *Smart Materials and Structures,* vol. 20, p. 045004, 2011.

[16] L. Tang, Y. Yang and C. Soh, "Toward broadband vibration-based energy harvesting," *Journal of Intelligent Material Systems and Structures,* vol. 21, pp. 1867-1897, 2010.

[17] D. Zhu, M. Tudor and S. Beeby, "Strategies for increasing the operating frequency range of vibration energy harvesters: a review," *Measurement Science and Technology,* vol. 21, p. 022001, 2010.

[18] S. Roundy, P. Wright and J. Rabaey, "A study of low level vibrations as a power source for wireless sensor nodes," *Computer Communications,* vol. 26, pp. 1131-1144, 2003.

[19] N. DuToit, B. Wardle and S. Kim, "Design considerations for MEMS-scale piezoelectric mechanical vibration energy harvesters," *Integrated Ferroelectrics,* vol. 71, pp. 121-160, 2005.

[20] G. Sebald, H. Kuwano, D. Guyomar and B. Ducharne, "Experimental Duffing oscillator for broadband piezoelectric energy harvesting," *Smart Materials and Structures,* vol. 20, p. 102001, 2011.

[21] M. Umeda, K. Nakamura and S. Ueha, "Analysis of transformation of mechanical impact energy to electrical energy using a piezoelectric vibrator," *Japan. J. Appl. Phys.,* Vols. 3267-73, p. 35, 1996.

[22] L. Tang, Y. Yang and C. Soh, "Improving functionality of vibration energy harvesters using magnets," *Journal of Intelligent Material Systems and Structures,* vol. 23, pp. 1433-1449, 2012.

[23] M. Karami, J. Farmer and D. Inman, "Parametrically excited nonlinear piezoelectric compact wind turbine," *Renewable Energy,* vol. 50, pp. 977-987, 2013.

[24] M. Daqaq, R. Masana, A. Erturk and D. Quinn, "On the role of nonlinearities in vibratory energy harvesting: a critical review and discussion," *Applied Mechanics Reviews,* vol. 66, p. 040801, 2014.

[25] A. Wickenheiser and E. Garcia, "Broadband vibration-based energy harvesting improvement through frequency up-conversion by magnetic excitation," *Smart Materials and Structures*, vol. 19, p. 065020, 2010.

[26] P. Pillatsch, E. Yeatman and A. Holmes, "A scalable piezoelectric impulse-excited energy harvester for human body excitation," *Smart Materials and Structures*, vol. 21, p. 115018, 2012.

[27] R. Harne, C. Zhang, B. Li and K. Wang, "An analytical approach for predicting the energy capture and conversion by impulsively-excited bistable vibration energy harvesters," *Journal of Sound and Vibration*, vol. 373, pp. 205-222, 2016.

[28] B. Andò, S. Baglio and F. Maiorca, "Analysis of two dimensional, wide-band, bistable vibration energy harvester," *Sensors and Actuators*, vol. A: Physical 202, pp. 176-182, 2013.

[29] W. Su and J. Zu, "Design and development of a novel bi-directional piezoelectric energy harvester," *Smart Materials and Structures*, vol. 23, p. 095012, 2014.

[30] L. Virgin, Vibration of Axially Loaded Structures, Cambridge: Cambridge University Press, 2007.

[31] K. Young, P. Landecker and D. Villani, "An analytical soulution for the force between two magnetic dipoles," *Physical Seperation in Science and Engineering*, vol. 9, pp. 39-52, 1998.

[32] I. Kozinsky, H. Postma, I. Bargatin and M. Roukes, "Tuning nonlinearity, dynamic range, and frequency of nanomechanical resonators," *Applied Physics Letters*, vol. 88, p. 253101, 2006.

6 APPENDIX

6.1 Sample MATLAB code

Below is a sample of the MATLAB code used for numerical analysis to investigate the characteristics of the magnetically coupled nonlinear vibration energy harvesting system over wide range of the parameters of the energy harvesters.

```
%% nonlinear vibration energy harvesting system composed of two piezoelectric
beams
% coupled together via magnetic potentials positioned at their beam tips
% see schematic magnets_FBD_2017_7_27.svg for system configuration and
% 2017_07_27_magnetic_repulsion_energy_harvester_system.docx for equation
% system derivation

clear all;
% close all;
% clc;

warning off

%% set tolerances for runge-kutta ode45 numerical integration
v.reltol=1e-8;1e-7; % relative tolerance on ode45 1e-5 for DC circuits
v.abstol=1e-10;1e-9; % absolute tolerance on ode45 1e-8 for DC circuits

%% system parameters
% piezoelectric energy harvester parameters
v.mass_beam_1=0.003;0.00413; % [kg] harvester lumped mass contributed from
beam 1
% v.mass_magnet_1=.007; % [kg] harvester mass contributed from tip-positioned
magnet for beam 1
v.mass_beam_2=0.003;0.00413; % [kg] harvester lumped mass contributed from
beam 2
% v.mass_magnet_2=.007; % [kg] harvester mass contributed from tip-positioned
magnet for beam 2
v.k1_1=60;110; % [N/m] linear stiffness contributed from beam 1
v.k1_2=60;110; % [N/m] linear stiffness contributed from beam 2
v.k3_1=.8*v.k1_1*1.25e5;.1*v.k1_1*1.25e5; % [N/m^3] nonlinear stiffness
contributed from beam 1
v.k3_2=.8*v.k1_1*1.25e5; % [N/m^3] nonlinear stiffness contributed from beam
2
v.damp_1=0.008; % [N.s/m] damping constant contributed from mechanical losses
in beam 1 and fixturing
v.damp_2=0.008; % [N.s/m] damping constant contributed from mechanical losses
in beam 2 and fixturing
v.alpha_1=.045e-4:2e-4; % [N/V] electromechanical coupling factor for
piezoelectric beam 1 (2e-4 for 5H piezoelectric material)
v.alpha_2=.058e-4;2e-4;0.8e-4; % [N/V] electromechanical coupling factor for
piezoelectric beam 2 (2e-4 for 5H piezoelectric material)
v.Cp_1=.278e-9; % [F] capacitance of piezoelectric beam 1
v.Cp_2=.278e-9; % [F] capacitance of piezoelectric beam 2
v.release_disp=0.004; % [m] release distance from attractive magnet to magnet
2
v.release_disp_all=v.release_disp;linspace(-0.005,0.01,100); % [m] release
position of beam 2
```

```
v.ks=0;150;220; % [N/m] linear spring stiffness of shape memory alloy (SMA)
spring
v.ks_1=0;50;50;320; % [N/m] equlvalent linear spring stiffness of
displacement bias on beam 1

% storage circuit parameters
% v.Cr=2.2e-6;0.1e-6; % [F] capacitance of storage element in rectifier
circuit
v.vd=0.5; % [V] diode forward voltage drop

% magnet relevant parameters
v.mu_0=4*pi*1e-7; % [N/A^2] free permeability constant
v.M_1=1.18e6;1.25e6; % [A/m] magnetization of tip magnet 1
v.M_2=1.25e6;1.45e6; % [A/m] magnetization of tip magnet 2
v.M_3=1.25e6;1.5e6; % [A/m] magnetization of tip magnet 3
v.V_1=.25*.25*.5*(.0254^3); % [m^3] volume of magnet 1
v.V_2=.25*.25*.5*(.0254^3); % [m^3] volume of magnet 2
v.V_3=.25*.25*.5*(.0254^3); % [m^3] volume of magnet 3

v.rho_neodymium=7300; % [kg/m^3] density of neodymium magnets
v.mass_mag_1=v.rho_neodymium*v.V_1; % [kg] harvester mass contributed from
tip-positioned magnet for beam 1
v.mass_mag_2=v.rho_neodymium*v.V_2; % [kg] harvester mass contributed from
tip-positioned magnet for beam 2
v.mass_total_1=v.mass_beam_1+v.mass_mag_1; % [kg] total harvester mass for
beam 1
v.mass_total_2=v.mass_beam_2+v.mass_mag_2; % [kg] total harvester mass for
beam 2

% component spacing relevant parameters
v.L=25e-3; % [m] horizontal spacing between magnet 1 and magnet 2
v.H=18e-3; % [m] vertical spacing between magnet 2 and fixed magnet
v.delta=0;-3.5e-3;-3e-3; % [m] horizontal offset between resting length of ks
spring and magnet 2
v.delta_1=0;1.5e-3; % [m] vertical offset between resting length of ks_1
spring and magnet 1
v.cap_delta_1=1.5e-3;0.5e-3;1.5e-3;0.7e-3; % [m] offset between magnet 1 and
magnet 2
v.cap_delta_2=0;-1.6e-3;-2.25e-3;-1.85e-3; % [m] offset between magnet 2 and
magnet 3

%% parameter to vary
incs=1; % number of increments of parameter to consider
v.L_all=1e-3*linspace(50000,50000,incs); % [m] horizontal distance between
magnet 1 and 2
v.H_all=1e-3*linspace(18,18,incs); % [m] vertical distance between magnet 2
and 3
v.init_vel_all=linspace(0.1,0.35,incs);0.22*ones(1,incs);0.13*ones(1,incs);10
e-2*logspace(0,1,incs);-1e-2*linspace(0.1,10,incs); % [m/s] initial impulse
on magnet 2 mass
v.Cr_all=.29e-6*ones(1,incs);linspace(1,10,incs)*1e-6;0.1e-6; % [F]
capacitance of storage element in rectifier circuit
tto=incs;

Rincs=1; % number of increments of resistance to consider
```

```
v.R_1_all=10e6;logspace(5,9,Rincs);10e6;1.2e5; % [Ohm] resistance on
harvester 1
v.R_2_all=10e6;logspace(5,8,Rincs);10e6;1.2e5; % [Ohm] resistance on
harvester 2


runstatic=1; % run the statically stable equilibria computation?
plotequilibria=1; % plot the static equilibria?
plotforces=1; % plot the forces for the equilibria configurations
rundynamic=0; % run the simulation for dynamic impulse response?
numsimruns=8; % number of times to run for different initial conditions
plotdynamicsweep=0; % plot the results of a dynamic simulation parameter
sweep?
videogo=0; % make 1a video?
plot_time_trunc=0;
%% runstatic? equilibria
if runstatic==1
%%
for ooo=1:tto
  v.L=v.L_all(ooo);
  v.H=v.H_all(ooo);
  v.Cr=v.Cr_all(ooo);
%% identify equilibria and stable equilibria
sol_trys=80;
ase=nan(2,sol_trys);
ause=nan(2,sol_trys);
options=optimoptions('fsolve','display','off','tolfun',1e-5);
parfor iii=1:sol_trys; % solve static equilibria equation
  % derived
2017_07_21_nonlinear_energy_harvester_magnetic_repulsion_forces_1.nb
  F21=@(x)3*v.mu_0*v.M_1*v.V_1*v.M_2*v.V_2/4/pi*(x(1)+v.cap_delta_1)*(-
2*(x(1)+v.cap_delta_1)^2+3*(v.L+x(2)+v.cap_delta_2)^2)./((x(1)+v.cap_delta_1)
^2+(v.L+x(2)+v.cap_delta_2)^2).^(7/2);
  F31=@(x)3*v.mu_0*v.M_1*v.V_1*v.M_3*v.V_3/4/pi*(-v.H+x(1)+v.cap_delta_1)*(-
3*v.L^2+2*(-v.H+x(1)+v.cap_delta_1)^2)./(v.L^2+(-
v.H+x(1)+v.cap_delta_1)^2).^(7/2);
  F12=@(x)3*v.mu_0*v.M_1*v.V_1*v.M_2*v.V_2/4/pi*(v.L+x(2)+v.cap_delta_2)*(-
4*(x(1)+v.cap_delta_1)^2+(v.L+x(2)+v.cap_delta_2)^2)./((x(1)+v.cap_delta_1)^2
+(v.L+x(2)+v.cap_delta_2)^2).^(7/2);
  F32=@(x)3*v.mu_0*v.M_2*v.V_2*v.M_3*v.V_3/4/pi*(x(2)+v.cap_delta_2)*(-
(x(2)+v.cap_delta_2)^2+4*v.H^2)./((x(2)+v.cap_delta_2)^2+v.H^2).^(7/2);


  g=@(x)[v.k1_1*x(1)+v.k3_1*x(1)^3-F21(x)-F31(x);v.k1_2*x(2)+v.k3_2*x(2)^3-
F32(x)-F12(x)];

  [xx,fval,exitflag]=fsolve(g,10e-3*randn(2,1),options);
  if exitflag==1
  se=xx; % assign fsolve output
  x_temp_1=se(1)+v.cap_delta_1;
  x_temp_2=v.L+se(2)+v.cap_delta_2;
% comp_gradient=[v.k1_1+3*v.k3_1*se(1)^2-3*v.M_1*v.M_2*v.V_1*v.V_2*v.mu_0*(-
4*x_temp_1^2*(x_temp_1^2+x_temp_2^2)-7*x_temp_1^2*(-
2*x_temp_1^2+3*x_temp_2^2)+(x_temp_1^2+x_temp_2^2)*(-
2*x_temp_1^2+3*x_temp_2^2))/4/pi/(x_temp_1^2+x_temp_2^2)^(9/2)
15*v.M_1*v.M_2*v.V_1*v.V_2*v.mu_0*x_temp_1*x_temp_2*(-
```

```
4*x_temp_1^2+3*x_temp_2^2)/4/pi/(x_temp_1^2+x_temp_2^2)^(9/2);15*v.M_1*v.M_2*
v.V_1*v.V_2*v.mu_0*x_temp_1*x_temp_2*(-
4*x_temp_1^2+3*x_temp_2^2)/4/pi/(x_temp_1^2+x_temp_2^2)^(9/2)
v.k1_2+3*v.k3_2*se(2)^2-3*v.M_1*v.M_2*v.V_1*v.V_2*v.mu_0*(-7*x_temp_2^2*(-
4*x_temp_1^2+x_temp_2^2)+2*x_temp_2^2*(x_temp_1^2+x_temp_2^2)+(-
4*x_temp_1^2+x_temp_2^2)*(x_temp_1^2+x_temp_2^2))/4/pi/(x_temp_1^2+x_temp_2^2
)^(9/2)-3*v.M_2*v.M_3*v.V_2*v.V_3*v.mu_0*(4*v.H^4-
27*v.H^2*(se(2)+v.cap_delta_2)^2+4*(se(2)+v.cap_delta_2)^4)/4/pi/(v.H^2+(se(2
)+v.cap_delta_2)^2)^(9/2)];
  comp_gradient=[v.k1_1+3*v.k3_1*se(1)^2-3*v.M_1*v.M_2*v.V_1*v.V_2*v.mu_0*(-
4*x_temp_1^2*(x_temp_1^2+x_temp_2^2)-7*x_temp_1^2*(-
2*x_temp_1^2+3*x_temp_2^2)+(x_temp_1^2+x_temp_2^2)*(-
2*x_temp_1^2+3*x_temp_2^2))/4/pi/(x_temp_1^2+x_temp_2^2)^(9/2)+3*v.M_1*v.M_3*
v.V_1*v.V_3*v.mu_0*(8*v.H^4+3*v.L^4-32*v.H^3*x_temp_1-
24*v.L^2*x_temp_1^2+8*x_temp_1^4-24*v.H^2*(v.L^2-2*x_temp_1^2)-
16*v.H*x_temp_1*(-3*v.L^2+2*x_temp_1^2))/4/pi/(v.L^2+(-v.H+x_temp_1)^2)^(9/2)
15*v.M_1*v.M_2*v.V_1*v.V_2*v.mu_0*x_temp_1*x_temp_2*(-
4*x_temp_1^2+3*x_temp_2^2)/4/pi/(x_temp_1^2+x_temp_2^2)^(9/2);15*v.M_1*v.M_2*
v.V_1*v.V_2*v.mu_0*x_temp_1*x_temp_2*(-
4*x_temp_1^2+3*x_temp_2^2)/4/pi/(x_temp_1^2+x_temp_2^2)^(9/2)
v.k1_2+3*v.k3_2*se(2)^2-3*v.M_1*v.M_2*v.V_1*v.V_2*v.mu_0*(-7*x_temp_2^2*(-
4*x_temp_1^2+x_temp_2^2)+2*x_temp_2^2*(x_temp_1^2+x_temp_2^2)+(-
4*x_temp_1^2+x_temp_2^2)*(x_temp_1^2+x_temp_2^2))/4/pi/(x_temp_1^2+x_temp_2^2
)^(9/2)-3*v.M_2*v.M_3*v.V_2*v.V_3*v.mu_0*(4*v.H^4-
27*v.H^2*(se(2)+v.cap_delta_2)^2+4*(se(2)+v.cap_delta_2)^4)/4/pi/(v.H^2+(se(2
)+v.cap_delta_2)^2)^(9/2)];

  % to neglect stable equilibria evaluation, COMMENT if,else,se statement
following, and end
  if det(comp_gradient)>0&&(comp_gradient(1,1)>0&&comp_gradient(2,2)>0) %
COMMENT to neglect stable equilibria evaluation
  ase(:,iii)=xx; % the equilibria are


  else % COMMENT to neglect stable equilibria evaluation
%    ause(:,iii)=xx; % the unstable equilibria are % COMMENT to neglect
stable equilibria evaluation
    ase(:,iii)=nan(2,1);
  end % COMMENT to neglect stable equilibria evaluation

  end

end

ase=ase'; % need to transpose for sake of computation
ause=ause'; % need to transpose for sake of computation

%%
% determining unique solutions, remainder are set to nan
wght=4; % # of sig figs must be unique to hold data
tmp=unique(10^(-wght)*round(10^(wght)*ase),'rows','stable');
ase=[tmp;nan(size(ase,1)-size(tmp,1),2)]; % uniquely determined static stable
equilibria
tmp=unique(10^(-wght)*round(10^(wght)*ause),'rows','stable');
```

```
ause=[tmp;nan(size(ause,1)-size(tmp,1),2)]; % uniquely determined static
unstable equilibria

%%
ase_out(:,:,ooo)=ase;
ause_out(:,:,ooo)=ause;
%%
for iii=1:sol_trys;
if isnan(ase_out(iii,1))==0 % for each stable equilibria
 x_temp_1=ase_out(iii,1)+v.cap_delta_1; % define temprary varible 1
 x_temp_2=v.L+ase_out(iii,2)+v.cap_delta_2; % define temprary varible 2
 jaco_1=1/v.mass_total_1*[0 v.mass_total_1;-v.k1_1-
3*v.k3_1*ase_out(iii,1)^2+3*v.M_1*v.M_2*v.V_1*v.V_2*v.mu_0*(-
4*x_temp_1^2*(x_temp_1^2+x_temp_2^2)-7*x_temp_1^2*(-
2*x_temp_1^2+3*x_temp_2^2)+(x_temp_1^2+x_temp_2^2)*(-
2*x_temp_1^2+3*x_temp_2^2))/4/pi/(x_temp_1^2+x_temp_2^2)^(9/2)-
(3*v.M_1*v.M_3*v.V_1*v.V_3*v.mu_0*(8*v.H^4+3*v.L^4-32*v.H^3*x_temp_1-
24*v.L^2*x_temp_1^2+8*x_temp_1^4-24*v.H^2*(v.L^2-2*x_temp_1^2)-
16*v.H*x_temp_1*(-3*v.L^2+2*x_temp_1^2))/4/pi/(v.L^2+(-
v.H+x_temp_1)^2)^(9/2)) -v.damp_1]; % Jacobian of beam 1
%  jaco_1=1/v.mass_total_1*[0 v.mass_total_1;-v.k1_1-
3*v.k3_1*ase_out(iii,1)^2+3*v.M_1*v.M_2*v.V_1*v.V_2*v.mu_0*(-
4*x_temp_1^2*(x_temp_1^2+x_temp_2^2)-7*x_temp_1^2*(-
2*x_temp_1^2+3*x_temp_2^2)+(x_temp_1^2+x_temp_2^2)*(-
2*x_temp_1^2+3*x_temp_2^2))/4/pi/(x_temp_1^2+x_temp_2^2)^(9/2) -v.damp_1]; %
Jacobian of beam 1

 lamda_11=0.5*(jaco_1(1,1)+jaco_1(2,2)-sqrt((jaco_1(1,1)+jaco_1(2,2))^2-
4*det(jaco_1))); % eigenvalue 1 of beam 1
 lamda_12=0.5*(jaco_1(1,1)+jaco_1(2,2)+sqrt((jaco_1(1,1)+jaco_1(2,2))^2-
4*det(jaco_1))); % eigenvalue 2 of beam 1
 jaco_2=1/v.mass_total_2*[0 v.mass_total_2;-v.k1_2-
3*v.k3_2*ase_out(iii,2)^2+3*v.M_1*v.M_2*v.V_1*v.V_2*v.mu_0*(-7*x_temp_2^2*(-
4*x_temp_1^2+x_temp_2^2)+2*x_temp_2^2*(x_temp_1^2+x_temp_2^2)+(-
4*x_temp_1^2+x_temp_2^2)*(x_temp_1^2+x_temp_2^2))/4/pi/(x_temp_1^2+x_temp_2^2
)^(9/2)+3*v.M_2*v.M_3*v.V_2*v.V_3*v.mu_0*(4*v.H^4-
27*v.H^2*(ase_out(iii,2)+v.cap_delta_2)^2+4*(ase_out(iii,2)+v.cap_delta_2)^4)
/4/pi/(v.H^2+(ase_out(iii,2)+v.cap_delta_2)^2)^(9/2) -v.damp_2]; % Jacobian
of beam 2
 lamda_21=0.5*(jaco_2(1,1)+jaco_2(2,2)-sqrt((jaco_2(1,1)+jaco_2(2,2))^2-
4*det(jaco_2))); % eigenvalue 1 of beam 2
 lamda_22=0.5*(jaco_2(1,1)+jaco_2(2,2)+sqrt((jaco_2(1,1)+jaco_2(2,2))^2-
4*det(jaco_2))); % eigenvalue 2 of beam 2
 fn_1(iii,ooo)=abs(imag(lamda_11))/2/pi; % [Hz] natrual frequency of beam 1
 fn_2(iii,ooo)=abs(imag(lamda_21))/2/pi; % [Hz] natrual frequency of beam 2
end
% fn_1_out(iii)=fn_1;
% fn_2_out(iii)=fn_2;
end
%%
end

%%
%% plot
colors=['r' 'g' 'b' 'c' 'm' 'k' 'r' 'g' 'b' 'c' 'm' 'k' 'r' 'g' 'b' 'c' 'm'
'k' 'r' 'g' 'b' 'c' 'm' 'k' 'r' 'g' 'b' 'c' 'm' 'k' 'r' 'g' 'b' 'c' 'm' 'k'
```

```
'r' 'g' 'b' 'c' 'm' 'k' 'r' 'g' 'b' 'c' 'm' 'k' 'r' 'g' 'b' 'c' 'm' 'k' 'r'
'g' 'b' 'c' 'm' 'k' 'r' 'g' 'b' 'c' 'm' 'k' 'r' 'g' 'b' 'c' 'm' 'k' 'r' 'g'
'b' 'c' 'm' 'k' 'r' 'g' 'b' 'c' 'm' 'k' 'r' 'g' 'b' 'c' 'm' 'k' 'r' 'g' 'b'
'c' 'm' 'k' 'r' 'g' 'b' 'c' 'm' 'k' 'r' 'g' 'b' 'c' 'm' 'k' 'r' 'g' 'b' 'c'
'm' 'k' 'r' 'g' 'b' 'c' 'm' 'k' 'r' 'g' 'b' 'c' 'm' 'k' 'r' 'g' 'b' 'c' 'm'
'k' 'r' 'g' 'b' 'c' 'm' 'k' 'r' 'g' 'b' 'c' 'm' 'k' 'r' 'g' 'b' 'c' 'm' 'k'
'r' 'g' 'b' 'c' 'm' 'k' 'r' 'g' 'b' 'c' 'm' 'k' 'r' 'g' 'b' 'c' 'm' 'k' 'r'
'g' 'b' 'c' 'm' 'k' 'r' 'g' 'b' 'c' 'm' 'k' 'r' 'g' 'b' 'c' 'm' 'k' 'r' 'g'
'b' 'c' 'm' 'k' 'r' 'g' 'b' 'c' 'm' 'k' 'r' 'g' 'b' 'c' 'm' 'k' 'r' 'g' 'b'
'c' 'm' 'k' 'r' 'g' 'b' 'c' 'm' 'k' 'r' 'g' 'b' 'c' 'm' 'k' 'r' 'g' 'b' 'c'
'm' 'k' 'r' 'g' 'b' 'c' 'm' 'k' 'r' 'g' 'b' 'c' 'm' 'k' 'r' 'g' 'b' 'c' 'm'
'k' 'r' 'g' 'b' 'c' 'm' 'k' 'r' 'g' 'b' 'c' 'm' 'k' 'r' 'g' 'b' 'c' 'm' 'k'
'r' 'g' 'b' 'c' 'm' 'k' 'r' 'g' 'b' 'c' 'm' 'k' 'r' 'g' 'b' 'c' 'm' 'k' 'r'
'g' 'b' 'c' 'm' 'k' ]; % colors preallocate
markers=['o' 's' 'v' 'd' '^' 'o' 's' 'v' 'd' '^' 'o' 's' 'v' 'd' '^' 'o' 's'
'v' 'd' '^' 'o' 's' 'v' 'd' '^' 'o' 's' 'v' 'd' '^' 'o' 's' 'v' 'd' '^' 'o'
's' 'v' 'd' '^' 'o' 's' 'v' 'd' '^' 'o' 's' 'v' 'd' '^' 'o' 's' 'v' 'd' '^'
'o' 's' 'v' 'd' '^' 'o' 's' 'v' 'd' '^' 'o' 's' 'v' 'd' '^' 'o' 's' 'v' 'd'
'^' 'o' 's' 'v' 'd' '^' 'o' 's' 'v' 'd' '^' 'o' 's' 'v' 'd' '^' 'o' 's' 'v'
'd' '^' 'o' 's' 'v' 'd' '^' 'o' 's' 'v' 'd' '^' 'o' 's' 'v' 'd' '^' 'o' 's'
'v' 'd' '^' 'o' 's' 'v' 'd' '^' 'o' 's' 'v' 'd' '^' 'o' 's' 'v' 'd' '^' 'o'
's' 'v' 'd' '^' 'o' 's' 'v' 'd' '^' 'o' 's' 'v' 'd' '^' 'o' 's' 'v' 'd' '^'
'o' 's' 'v' 'd' '^' 'o' 's' 'v' 'd' '^' 'o' 's' 'v' 'd' '^' 'o' 's' 'v' 'd'
'^' 'o' 's' 'v' 'd' '^' 'o' 's' 'v' 'd' '^' 'o' 's' 'v' 'd' '^' 'o' 's' 'v'
'd' '^' 'o' 's' 'v' 'd' '^' 'o' 's' 'v' 'd' '^' 'o' 's' 'v' 'd' '^' 'o' 's'
'v' 'd' '^' 'o' 's' 'v' 'd' '^' 'o' 's' 'v' 'd' '^' 'o' 's' 'v' 'd' '^' ]; %
markers preallocate

if plotequilibria==1
figure(1);
clf;
hold on
for iii=1:size(ase_out,1)
% plot3(-
v.L_all.*ones(tto,1)'*1e3,[1:tto]',squeeze(ase_out(iii,1,:))*1e3,[colors(iii)
'o']);
% plot3(squeeze(ase_out(iii,2,:))*1e3,[1:tto]',0.*ones(tto,1),[colors(iii)
's']);

plot3(-
v.L_all.*ones(tto,1)'*1e3,[1:tto]',squeeze(ase_out(iii,1,:))*1e3+v.cap_delta_
1*1e3,['ro']);
plot3(squeeze(ase_out(iii,2,:))*1e3+v.cap_delta_2*1e3,[1:tto]',0.*ones(tto,1)
,['rs']);
plot3(-
v.L_all.*ones(tto,1)'*1e3,[1:tto]',squeeze(ause_out(iii,1,:))*1e3,['go']);
plot3(squeeze(ause_out(iii,2,:))*1e3,[1:tto]',0.*ones(tto,1),['gs']);

end
plot3(0.*ones(tto,1)',[1:tto]',v.H_all*1e3,'ok','markerfacecolor','k');
% plot3(0.*ones(tto,1)',[1:tto]',v.H_all,'k');
```

```
box on
% axis(1e-3*[-25 15 -25 25]);
% axis equal
% axis([min(-v.L_all.*ones(tto,1)') max(max(-squeeze(ase_out(:,2,:)))) 1 tto
min(min(squeeze(ase_out(:,1,:)))) max(v.H_all)])
xlabel('i [mm]');
ylabel('parameter change');
zlabel('j [mm]');
view([-45 40])
grid on;
titlename1=['k1_1=' num2str(v.k1_1) '. k1_2=' num2str(v.k1_2) '. k3_1='
num2str(v.k3_1,'%10.1e') '. k3_2=' num2str(v.k3_2,'%10.1e') '. alpha_1='
num2str(v.alpha_1,'%10.1e') '. alpha_2=' num2str(v.alpha_2,'%10.1e')];
% titlename2=['k_s=' num2str(v.ks) '. k_s1=' num2str(v.ks_1) '. delta='
num2str(v.delta) '. delta1=' num2str(v.delta_1) '. M_1='
num2str(v.M_1,'%10.1e') '. M_2=' num2str(v.M_2,'%10.1e') '. M_3='
num2str(v.M_3,'%10.1e')];
titlename2=['delta_1=' num2str(v.cap_delta_1) '. delta_2='
num2str(v.cap_delta_2) '. M_1=' num2str(v.M_1,'%10.1e') '. M_2='
num2str(v.M_2,'%10.1e') '. M_3=' num2str(v.M_3,'%10.1e')];
titlename3=['min L=' num2str(min(v.L_all)) '. max L=' num2str(max(v.L_all))
'. min H=' num2str(min(v.H_all)) '. max H=' num2str(max(v.H_all))];
titlename4=['L=' num2str(min(v.L_all)) ' H=' num2str(min(v.H_all))];
title({titlename1,titlename2,titlename3});
end

%% plot the potential energy and/or force profiles as functions of
displacement coordinates
if plotforces==1
% create ordinary sorted stable equilibria vectors
temp_ase_out=[];
for ooo=1:tto
  temp_ase_out(:,1,ooo)=sort(squeeze(ase_out(:,1,ooo)));
  temp_ase_out(:,2,ooo)=sort(squeeze(ase_out(:,2,ooo)));
end

equilibria_1=1; % which equilibria for beam 1 to evaluate different beam 2
positions over
equilibria_2=1; % which equilibria for beam 2 to evaluate different beam 1
positions over

% preallocate
force_1=[];force_2=[];
potential_1=[];potential_2=[];

% set range of displacements and zero-dummy vectors
x1=10e-3*linspace(-1,1,101);
x2_1=zeros(size(x1));
x2=10e-3*linspace(-1,1,101);
x1_2=zeros(size(x2));

% for all L and H combinations, compute force and potentials
for ooo=1:tto
  force1=[];
  force2=[];
for ppp=1:length(x1)
```

```
v.L=v.L_all(ooo);
v.H=v.H_all(ooo);

F21=@(x)3*v.mu_0*v.M_1*v.V_1*v.M_2*v.V_2/4/pi*(x(1)+v.cap_delta_1)*(-
2*(x(1)+v.cap_delta_1)^2+3*(v.L+x(2)+v.cap_delta_2)^2)./((x(1)+v.cap_delta_1)
^2+(v.L+x(2)+v.cap_delta_2)^2).^(7/2);
F31=@(x)3*v.mu_0*v.M_1*v.V_1*v.M_3*v.V_3/4/pi*(-v.H+x(1)+v.cap_delta_1)*(-
3*v.L^2+2*(-v.H+x(1)+v.cap_delta_1)^2)./(v.L^2+(-
v.H+x(1)+v.cap_delta_1)^2).^(7/2);
F12=@(x)3*v.mu_0*v.M_1*v.V_1*v.M_2*v.V_2/4/pi*(v.L+x(2)+v.cap_delta_2)*(-
4*(x(1)+v.cap_delta_1)^2+(v.L+x(2)+v.cap_delta_2)^2)./((x(1)+v.cap_delta_1)^2
+(v.L+x(2)+v.cap_delta_2)^2).^(7/2);
F32=@(x)3*v.mu_0*v.M_2*v.V_2*v.M_3*v.V_3/4/pi*(x(2)+v.cap_delta_2)*(-
(x(2)+v.cap_delta_2)^2+4*v.H^2)./((x(2)+v.cap_delta_2)^2+v.H^2).^(7/2);


g1=@(x)[v.k1_1*x(1)+v.k3_1*x(1)^3-F21(x)-F31(x)];
g2=@(x)[v.k1_2*x(2)+v.k3_2*x(2)^3-F32(x)-F12(x)];

force1(ppp)=g1([x1(ppp) x2_1(ppp)]);
force2(ppp)=g2([x1_2(ppp) x2(ppp)]);

force1(ppp)=g1([x1(ppp) temp_ase_out(equilibria_2,2,ooo)]);
force2(ppp)=g2([temp_ase_out(equilibria_1,1,ooo) x2(ppp)]);

end
force_1(:,ooo)=force1;
force_2(:,ooo)=force2;
potential_1(:,ooo)=cumtrapz(x1,force1);
potential_2(:,ooo)=cumtrapz(x2,force2);
end
ahold1=min(min(potential_1));
ahold2=min(min(potential_2));
%%
figure(3);
% clf;
for ooo=1:tto
% plot3(1e3*x1,1e0*ooo*ones(size(x1)),1e2*potential_1(:,ooo)-1e2*ahold1,'r');
hold on
% plot3(1e3*x2+v.cap_delta_2*1e3,1e0*ooo*ones(size(x2)),potential_2(:,ooo)-
ahold2,'b');
end
grid on
box on
% xlabel('i [mm]')
xlabel('i [mm]')
% zlabel('potential energy [J]. red, 100x beam 1. blue, beam 2.')
zlabel('potential energy [J]')
xlim([-6,6])
zlim([0 1.5e-3])
view(0,0)
% title({titlename4});

figure(4);
clf;
```

```
for ooo=1:tto
% plot3(1e3*x1,1e0*ooo*ones(size(x1)),5e0*force_1(:,ooo)-0e0*ahold1,'r');
hold on
plot3(1e3*x2+v.cap_delta_2*1e3,1e0*ooo*ones(size(x2)),force_2(:,ooo)-
0*ahold2,'--r');
end
grid on
view(0,0)
xlim([-5,5])
box on
xlabel('i [mm]')
ylabel('j [mm]')
% zlabel('force [N]. red, 50x beam 1. blue, beam 2.')
zlabel('force [N]. blue, beam 2.')
title({titlename1,titlename2,titlename3});

end

%%
%%
end

%% rundynamic? perturbation
if rundynamic==1
%% simulate impulse response of harvesters due to initial velocity on the
magnet2/beam2 sub-system

%% determining runtime operating parameters

% if length(v.R_1_all)==1
% ttp=length(v.alpha_all);
% else
ttp=length(v.R_1_all);
% end

%% preallocate
init_pot_energy_drop=nan(tto,ttp,numsimruns,2); % initial potential energy of
sub-systems
max_mech_energy_drop=nan(tto,ttp,numsimruns,2); % maximum mechanical energy
of sub-systems
tot_mech_energy_drop=nan(tto,ttp,numsimruns,2); % total energy of sub-systems
max_elec_power_drop=nan(tto,ttp,numsimruns,2); % maximum electric power
generated
tot_elec_energy_drop=nan(tto,ttp,numsimruns,2); % total electric energy
generated
net_trans_force_drop=nan(tto,ttp,numsimruns,2); % total net force transmitted
to base
net_ini_trans_force_drop=nan(tto,ttp,numsimruns,2); % total initial net force
transmitted to base
%%
tic
for ppp=1:ttp % for either R or alpha parameter
    %%
% if length(v.R_1_all)==1
% v.alpha=v.alpha_all(ppp);
% v.R=v.R_all(1);
```

```
% else
% v.alpha=v.alpha_all(1);
v.R_1=v.R_1_all(ppp); % assign instantaneous load resistance value
v.R_2=v.R_2_all(ppp); % assign instantaneous load resistance value
% end

%%
% z=v; % hold structure

%%
for ooo=1:tto % par
%%
% v=struct();
% v=z; % remake structure

  %%
v.L=v.L_all(ooo);
v.H=v.H_all(ooo);
v.init_vel=v.init_vel_all(ooo);
v.Cr=v.Cr_all(ooo);

%%
%%
% set the number of runtime periods according to the haronic natural
frequency due to expediting computations
fs=2048; % samples per excitation period
v.omega=sqrt(1*(v.k1_2)/(v.mass_beam_2+v.mass_mag_2)); % linear natural
frequency of beam 2 without magnetic forces
v.periods=100;3/(2*pi/v.omega); % number of periods to numerically integrate
over
v.omega_1=sqrt(1*(v.k1_1)/(v.mass_beam_1+v.mass_mag_1)); % linear natural
frequency of beam 1 without magnetic forces
v.time=0:1/fs*2*pi/v.omega:v.periods*2*pi/v.omega; % create time vector
v.w=zeros(size(v.time)); % [m/s^2] standard deviation of harmonic base
acceleration

%% preallocate
init_pot_energy_1=nan(numsimruns,1);
init_pot_energy_2=nan(numsimruns,1);
max_mech_energy_1=nan(numsimruns,1);
max_mech_energy_2=nan(numsimruns,1);
tot_mech_energy_1=nan(numsimruns,1);
tot_mech_energy_2=nan(numsimruns,1);
max_elec_power_1=nan(numsimruns,1);
max_elec_power_2=nan(numsimruns,1);
tot_elec_energy_1=nan(numsimruns,1);
tot_elec_energy_2=nan(numsimruns,1);

%%
z=v; % hold structure

%%
parfor eee=1:numsimruns % par
%%
% tic
```

```
%%
v=struct();
v=z; % remake structure

%% set start parameters for simulation initial conditions
random_integer=randi(6);
init_c=[ase_out(random_integer,1,ooo)*(1+1e-1*randn) 1e-4*randn
ase_out(random_integer,2,ooo)*(1+1e-1*randn) v.init_vel*(-1) zeros(1,4)]; %
initial conditions of displacement, velocity, voltages
% init_c=[ase_out(random_integer,1,ooo)*(1+1e-1*randn) v.init_vel*(-1)
ase_out(random_integer,2,ooo)*(1+1e-1*randn) 1e-4*randn zeros(1,4)]; %
initial conditions of displacement, velocity, voltages
% init_c=[temp_ase_out(equilibria_1,1,1) 1e-4*randn v.release_disp 1e-4*randn
zeros(1,4)]; % initial conditions of displacement, velocity, voltages
while
isnan(ase_out(random_integer,1,ooo))==1||isnan(ase_out(random_integer,2,ooo))
==1
  random_integer=randi(6);
  init_c=[ase_out(random_integer,1,ooo)*(1+1e-1*randn) 1e-4*randn
ase_out(random_integer,2,ooo)*(1+1e-1*randn) v.init_vel*(-1) zeros(1,4)]; %
initial conditions of displacement, velocity, voltages
%  init_c=[ase_out(random_integer,1,ooo)*(1+1e-1*randn) v.init_vel*(-1)
ase_out(random_integer,2,ooo)*(1+1e-1*randn) 1e-4*randn zeros(1,4)]; %
initial conditions of displacement, velocity, voltages
  % init_c=[temp_ase_out(equilibria_1,1,1) 1e-4*randn v.release_disp 1e-
4*randn zeros(1,4)]; % initial conditions of displacement, velocity, voltages
end
v.init_c=init_c;

%
options=odeset('reltol',v.reltol,'abstol',v.abstol,'events',@(t,x)events_nonl
inear_harvester_magnetic_repulsion_dynamic_run_4(t,x,v));
%
[t,y,te,ye,ie]=ode45(@(t,x)energy_harvester_nonlinear_circuit_dc_funcsim_7(t,
x,v),v.time,init_c,options);

options=odeset('reltol',v.reltol,'abstol',v.abstol);
[t,y]=ode45(@(t,x)energy_harvester_nonlinear_circuit_dc_funcsim_10(t,x,v),v.t
ime,init_c,options);

for aaa=1:length(y(:,7))
  if y(aaa,7)<=-2
   y(aaa,7)=0;
  end
  if y(aaa,8)<=0
   y(aaa,8)=0;
  end
end

%%
% grab data for beams
if isnan(y(end,1))~=1
init_pot_energy_1(eee)=1/2*v.k1_1*y(1,1).^2+1/4*v.k3_1*y(1,1).^4+1/2*v.ks_1*(
y(1,1)-v.delta_1).^2+v.M_1*v.M_2*v.V_1*v.V_2*(-
```

```
y(1,1).^2+2*(v.L+y(1,3)).^2*v.mu_0/4/pi/(y(1,1).^2+(v.L+y(1,3)).^2).^(5/2));
% initial potential energy for beam 1
init_pot_energy_2(eee)=1/2*v.k1_2*y(1,3).^2+1/4*v.k3_2*y(1,3).^4+1/2*v.ks*(y(
1,3)-
v.delta).^2+v.M_1*v.M_2*v.V_1*v.V_2*v.mu_0*(y(1,1).^2+2*(v.L+y(1,3)).^2)/4/pi
/(y(1,1).^2+(v.L+y(1,3)).^2).^(5/2)+v.M_2*v.M_3*v.V_2*v.V_3*v.mu_0*(v.H^2-
2*y(1,3).^2)/4/pi/(v.H^2+y(1,3).^2).^(5/2); % initial potential energy for
beam 2
max_mech_energy_1(eee)=1/2*(v.mass_beam_1+v.mass_mag_1)*max(abs(y(:,2))).^2;
% max kinetic energy for beam 1
max_mech_energy_2(eee)=1/2*(v.mass_beam_2+v.mass_mag_2)*max(abs(y(:,4))).^2;
% max kinetic energy for beam 2
temp=(v.mass_beam_1+v.mass_mag_1)*trapz(t,abs(y(:,2)).^2);
tot_mech_energy_1(eee)=temp(end); % total energy for beam 1
temp=(v.mass_beam_2+v.mass_mag_2)*trapz(t,abs(y(:,4)).^2);
tot_mech_energy_2(eee)=temp(end); % total energy for beam 2
max_elec_power_1(eee)=1/2*max(abs(y(:,7)).^2)/v.R_1; % maximum instantaneous
electric power generated by beam 1
max_elec_power_2(eee)=1/2*max(abs(y(:,8)).^2)/v.R_2; % maximum instantaneous
electric power generated by beam 2
temp=trapz(t,abs(y(:,7)).^2)/v.R_1;
tot_elec_energy_1(eee)=temp(end); % total electric energy generated by beam -
2
temp=trapz(t,abs(y(:,8)).^2)/v.R_2;
tot_elec_energy_2(eee)=temp(end); % total electric energy generated by beam 2

f_1=v.damp_1*y(:,2)+v.k1_1*y(:,1); % [N] force transimitted from beam 1
f_2=v.damp_2*y(:,4)+v.k1_2*y(:,3); % [N] force transimitted from beam 2
f_3_i=3*v.mu_0*v.M_1*v.V_1*v.M_3*v.V_3*v.L/4/pi*(-v.L^2+4*(-
v.H+y(:,1)+v.cap_delta_1).^2)./(v.L^2+(-v.H+y(:,1)+v.cap_delta_1).^2).^(7/2)-
3*v.mu_0*v.M_2*v.V_2*v.M_3*v.V_3/4/pi.*(y(:,3)+v.cap_delta_2).*(4*v.H^2-
(y(:,3)+v.cap_delta_2).^2)./(v.H^2+(y(:,3)+v.cap_delta_2).^2).^(7/2); % [N]
force transimitted in i-direction from fixed magnet 3
f_3_j=-3*v.mu_0*v.M_1*v.V_1*v.M_3*v.V_3/4/pi*(-v.H+y(:,1)+v.cap_delta_1).*(-
3*v.L^2+2*(-v.H+y(:,1)+v.cap_delta_1).^2)./(v.L^2+(-
v.H+y(:,1)+v.cap_delta_1).^2).^(7/2)-
3*v.mu_0*v.M_2*v.V_2*v.M_3*v.V_3/4/pi*v.H*(-
2*v.H^2+3*(y(:,3)+v.cap_delta_2).^2)./((y(:,3)+v.cap_delta_2).^2+v.H^2).^(7/2
); % [N] force transimitted in j-direction from fixed magnet 3
f_i=f_2+f_3_i; % [N] net force in i-direction
f_j=f_1+f_3_j; % [N] net force in j-direction
f_i_d=f_i-(f_i(1)); % [N] dynamic force in i-direction
f_j_d=f_j-(f_j(1)); % [N] dynamic force in j-direction
f_i_ini(eee)=f_i(1); % [N] initial net force in i-direction
f_j_ini(eee)=f_j(1); % [N] initial net force in j-direction
f_i_max(eee)=max(abs(f_i_d)); % [N] max dynamic force in i-direction
f_j_max(eee)=max(abs(f_j_d)); % [N] max dynamic force in j-direction
end

%%
if plot_time_trunc==1
%%
titlename1=['k1_1=' num2str(v.k1_1) '. k1_2=' num2str(v.k1_2) '. k3_1='
num2str(v.k3_1,'%10.1e') '. k3_2=' num2str(v.k3_2,'%10.1e') '. alpha_1='
num2str(v.alpha_1,'%10.1e') '. alpha_2=' num2str(v.alpha_2,'%10.1e')];
```

```
% titlename2=['k_s=' num2str(v.ks) '. k_s1=' num2str(v.ks_1) '. delta='
num2str(v.delta) '. delta1=' num2str(v.delta_1) '. M_1='
num2str(v.M_1,'%10.1e') '. M_2=' num2str(v.M_2,'%10.1e') '. M_3='
num2str(v.M_3,'%10.1e')];
titlename2=['offset delta_1=' num2str(v.cap_delta_1) '. offset delta_2='
num2str(v.cap_delta_2) '. M_1=' num2str(v.M_1,'%10.1e') '. M_2='
num2str(v.M_2,'%10.1e') '. M_3=' num2str(v.M_3,'%10.1e')];
titlename3=['min L=' num2str(min(v.L_all)) '. max L=' num2str(max(v.L_all))
'. min H=' num2str(min(v.H_all)) '. max H=' num2str(max(v.H_all))];
titlename4=['min initial vel=' num2str(min(v.init_vel_all)) '. max initial
vel=' num2str(max(v.init_vel_all)) '. R_1=' num2str(v.R_1,'%10.1e') '. R_2='
num2str(v.R_2,'%10.1e')];
% titlename4=['beam 2 release position, x_2=' num2str(v.release_disp) '.
R_1=' num2str(v.R_1,'%10.1e') '. R_2=' num2str(v.R_2,'%10.1e')];

%
potential_initial=1/2*v.k1_2*init_c(3).^2+1/4*v.k3_2*init_c(3).^4+1/2*v.ks*(i
nit_c(3)-v.delta).^2;
potential_initial=1/2*v.k1_2*init_c(3).^2+1/4*v.k3_2*init_c(3).^4+1/2*v.ks*(i
nit_c(3)-v.delta).^2+v.M_1*v.M_2*v.mu_0*v.V_1*v.V_2.*(-
init_c(1).^2+2*(v.L+init_c(3)).^2)./4/pi./(init_c(1).^2+(v.L+init_c(3)).^2).^
(5/2)+v.M_2*v.M_3*v.V_2*v.V_3*v.mu_0*(v.H^2-
2*init_c(3).^2)./4/pi./(v.H^2+init_c(3).^2).^(5/2);
potential=1/2*v.k1_2*y(:,3).^2+1/4*v.k3_2*y(:,3).^4+1/2*v.ks*(y(:,3)-
v.delta).^2+v.M_1*v.M_2*v.mu_0*v.V_1*v.V_2.*(-
y(:,1).^2+2*(v.L+y(:,3)).^2)./4/pi./(y(:,1).^2+(v.L+y(:,3)).^2).^(5/2)+v.M_2*
v.M_3*v.V_2*v.V_3*v.mu_0*(v.H^2-2*y(:,3).^2)./4/pi./(v.H^2+y(:,3).^2).^(5/2);
kinetic_initial=1/2*(v.mass_beam_2+v.mass_mag_2)*init_c(4).^2;
kinetic=1/2*(v.mass_beam_2+v.mass_mag_2)*y(:,4).^2;

% v.delta=0;
% v.delta_1=0;
f_1=v.damp_1*y(:,2)+v.k1_1*y(:,1); % [N] force transimitted from beam 1
f_2=v.damp_2*y(:,4)+v.k1_2*y(:,3); % [N] force transimitted from beam 2
f_3_i=3*v.mu_0*v.M_1*v.V_1*v.M_3*v.V_3*v.L/4/pi*(-v.L^2+4*(-
v.H+y(:,1)+v.cap_delta_1).^2)./(v.L^2+(-v.H+y(:,1)+v.cap_delta_1).^2).^(7/2)-
3*v.mu_0*v.M_2*v.V_2*v.M_3*v.V_3/4/pi.*(y(:,3)+v.cap_delta_2).*(4*v.H^2-
(y(:,3)+v.cap_delta_2).^2)./(v.H^2+(y(:,3)+v.cap_delta_2).^2).^(7/2); % [N]
force transimitted in i-direction from fixed magnet 3
f_3_j=-3*v.mu_0*v.M_1*v.V_1*v.M_3*v.V_3/4/pi*(-v.H+y(:,1)+v.cap_delta_1).*(-
3*v.L^2+2*(-v.H+y(:,1)+v.cap_delta_1).^2)./(v.L^2+(-
v.H+y(:,1)+v.cap_delta_1).^2).^(7/2)-
3*v.mu_0*v.M_2*v.V_2*v.M_3*v.V_3/4/pi*v.H*(-
2*v.H^2+3*(y(:,3)+v.cap_delta_2).^2)./((y(:,3)+v.cap_delta_2).^2+v.H^2).^(7/2
); % [N] force transimitted in j-direction from fixed magnet 3
f_i=f_2+f_3_i; % [N] net force in i-direction
f_j=f_1+f_3_j; % [N] net force in j-direction
f_i_d=f_i-(f_i(1)); % [N] dynamic force in i-direction
f_j_d=f_j-(f_j(1)); % [N] dynamic force in j-direction

f_2_release=v.damp_2*0+v.k1_2*v.release_disp+v.ks*(v.release_disp-v.delta)-
3*v.mu_0*v.M_1*v.V_1*v.M_2*v.V_2/4/pi*(v.L+v.release_disp).*(-
3*v.delta_1^2+2*(v.L+v.release_disp).^2)./(v.delta_1^2+(v.L+v.release_disp).^
2).^(7/2)-3*v.mu_0*v.M_2*v.V_2*v.M_3*v.V_3/4/pi*v.release_disp.*(-
2*v.release_disp.^2+3*v.H^2)./(v.release_disp.^2+v.H^2).^(7/2); % [N] force
when release beam 2figure(245);
```

```
clf
subplot(2,1,1)
hold on
% plot(t/(2*pi/v.omega),1e3*y(:,3),'-g');
% plot(t/(2*pi/v.omega),1e3*y(:,1),'r');
% xlim([min(t/(2*pi/v.omega)) max(t/(2*pi/v.omega))]);
plot(t,1e3*y(:,3),'-g');
plot(t,1e3*y(:,1),'-r');
% plot(t,gradient(y(:,3))./gradient(t),'-g');
% plot(t,gradient(y(:,1))./gradient(t),'-r');
% xlim([min(t) max(t)]);
xlim([0 2]);
ylim([-10 10]);
% xlabel('normalized periods in natural cycles')
xlabel('time [s]')
ylabel('red beam 1. green beam 2. displacement [mm]');
box on
title({titlename1,titlename2,titlename3,titlename4});
subplot(2,1,2)
hold on
% plot(t/(2*pi/v.omega),y(:,6),'-r');
% plot(t/(2*pi/v.omega),y(:,5),'c');
% plot(t/(2*pi/v.omega),y(:,7),'b');
% plot(t/(2*pi/v.omega),y(:,8),'-g');
% xlim([min(t/(2*pi/v.omega)) max(t/(2*pi/v.omega))]);
% plot(t,-gradient(y(:,3))./gradient(t),'g')
plot(t,y(:,6),'-g');
plot(t,y(:,5),'r');
plot(t,y(:,7),'b');
plot(t,y(:,8),'-c');
% xlim([0 max(t)]);
xlim([0 2]);
ylim([-3 3]);
box on
% xlabel('normalized periods in natural cycles')
xlabel('time [s]')
title({'red 1 transduced voltage [V]. blue beam 1 rectified voltage
[V]','green beam 2 transduced voltage [V]. cyon beam 2 rectified voltage
[V]'});




%%

end
%%
if videogo==1
  %%
% video file
loadname='filename'; % what filename
videoname=[loadname '.avi'];
writerobj=avifile(videoname,'quality',25,'fps',25);
figure(11);
clf;
set(gca,'nextplot','replacechildren');
```

```
trunc=1:40:length(t);
for iii=1:length(trunc)
  clf
  plot(-1e3*v.L,1e3*y(iii,1),'or','markerfacecolor','r')
  hold on
  plot(1e3*y(iii,3),0,'ob','markerfacecolor','b')
  plot(0,1e3*v.H,'ok','markerfacecolor','k');
  axis([-25 10 -10 10]);
  box on
  xlabel('x [mm]');
  ylabel('y [mm]');
  writerobj=addframe(writerobj,gcf);
end;
writerobj=close(writerobj);
%%
end

%%



%%
end
%%
%%
% store results for the given control parameter
init_pot_energy_drop(ooo,ppp,:,:)=[init_pot_energy_1 init_pot_energy_2];
max_mech_energy_drop(ooo,ppp,:,:)=[max_mech_energy_1 max_mech_energy_2];
tot_mech_energy_drop(ooo,ppp,:,:)=[tot_mech_energy_1 tot_mech_energy_2];
max_elec_power_drop(ooo,ppp,:,:)=[max_elec_power_1 max_elec_power_2];
tot_elec_energy_drop(ooo,ppp,:,:)=[tot_elec_energy_1 tot_elec_energy_2];
net_trans_force_drop(ooo,ppp,:,:)=[f_i_max' f_j_max'];
net_ini_trans_force_drop(ooo,ppp,:,:)=[f_i_ini' f_j_ini'];
%%
disp([num2str(ooo) ' of ' num2str(tto) '. ' num2str(ppp) ' of ' num2str(ttp)
''']);
%%

%%
end
%%
end
toc

%%
%% plot dynamic results from parameter sweep
if plotdynamicsweep==1
%%
R_to_plot=1; % which of the DC load resistance cases to plot
vel_to_plot=1; % which of the DC load resistance cases to plot
% figure(221);
% clf;
% hold on
% %
plot(1/2*(v.mass_beam_2+v.mass_mag_2)*v.init_vel_all.^2,squeeze(tot_elec_ener
gy_drop(:,R_to_plot,:,1)),[colors(1) markers(1)]);
```

```
% %
plot(1/2*(v.mass_beam_2+v.mass_mag_2)*v.init_vel_all.^2,squeeze(tot_elec_ener
gy_drop(:,R_to_plot,:,2)),[colors(2) markers(2)]);
%
plot(v.init_vel_all,squeeze(tot_elec_energy_drop(:,R_to_plot,:,1)),[colors(1)
markers(1)]);
%
plot(v.init_vel_all,squeeze(tot_elec_energy_drop(:,R_to_plot,:,2)),[colors(2)
markers(2)]);
% %
plot(1e3*v.L_all,squeeze(tot_elec_energy_drop(:,R_to_plot,:,1)),[colors(1)
markers(1)]);
% %
plot(1e3*v.L_all,squeeze(tot_elec_energy_drop(:,R_to_plot,:,2)),[colors(2)
markers(2)]);
% box on
% set(gca,'xscale','linear');
% set(gca,'yscale','linear');
% xlabel('initial velocity for beam 2 [m/s]');
% % xlabel('initial kinetic energy to beam 2 [J]');
% % xlabel('H [mm]');
% % xlabel('L [mm]');
ylabel({'red harvester 1. green harvester 2','total electric energy generated
[J]'})
titlename1=['k1_1=' num2str(v.k1_1) '. k1_2=' num2str(v.k1_2) '. k3_1='
num2str(v.k3_1,'%10.1e') '. k3_2=' num2str(v.k3_2,'%10.1e') '. alpha_1='
num2str(v.alpha_1,'%10.1e') '. alpha_2=' num2str(v.alpha_2,'%10.1e')];
titlename2=['k_s=' num2str(v.ks) '. k_s1=' num2str(v.ks_1) '. delta='
num2str(v.delta) '. delta1=' num2str(v.delta_1) '. M_1='
num2str(v.M_1,'%10.1e') '. M_2=' num2str(v.M_2,'%10.1e') '. M_3='
num2str(v.M_3,'%10.1e')];
titlename3=['min L=' num2str(min(v.L_all)) '. max L=' num2str(max(v.L_all))
'. min H=' num2str(min(v.H_all)) '. max H=' num2str(max(v.H_all))];
titlename4=['min initial vel=' num2str(min(v.init_vel_all)) '. max initial
vel=' num2str(max(v.init_vel_all)) '. R_1=' num2str(v.R_1,'%10.1e') '. R_2='
num2str(v.R_2,'%10.1e')];
titlename5=['L=' num2str(max(v.L_all)*1e3) '[mm] H='
num2str(min(v.H_all)*1e3) '[mm]'];
title(titlename5);


%%

end

%%
end
%%

%%
```